



# Bayesian Optimisation for Bio-based Biodegradable Aliphatic Polyester Thermosets

Thomas J Højlund-Dodd  
Hughes Hall  
University of Cambridge

*Principal Supervisor: Prof James Elliott  
Co-Supervisors: Prof Rachel Evans, Prof Alexei Lapkin*

*Submitted for PhD Progression  
Easter Term 2023*

## Table of Contents

<b><i>Chapter 1 – Rationale &amp; Literature Review.....</i></b>	<b>1</b>
<b>1.1 – Literature Review .....</b>	<b>1</b>
<b>1.2 – Report Overview .....</b>	<b>4</b>
<b><i>Chapter 2 – Research Completed .....</i></b>	<b>6</b>
<b>2.1 – Preliminary Experimental Work .....</b>	<b>7</b>
2.1.1 – Target Variable Identification .....	7
2.1.2 – Constant & Predictor Variable Identification .....	9
<b>2.2 – Optimisation Problem Framing .....</b>	<b>9</b>
2.2.1 – 1D Optimisation Problem for P(GIt).....	11
2.2.2 – 3D Optimisation Problem for P(GCiIt) .....	12
2.2.3 – 5D+ Optimisation Problems for Complex BBAPT Systems.....	14
<b>2.3 – Black-Box Function Evaluation Method.....</b>	<b>17</b>
<b>2.4 – Sequential Sampling Method .....</b>	<b>18</b>
2.4.1 – Bayesian Statistical Modelling Method.....	18
2.4.2 – Acquisition Function Method.....	20
<b>2.5 – P(GCiIt) System Optimisation .....</b>	<b>21</b>
2.5.1 – Theoretical Maximum Mass Loss .....	21
2.5.2 – Benchmarking Optimisations .....	22
2.5.3 – Bayesian Optimisations.....	23
2.5.4 – Cross-Comparison of Optimisations .....	24
<b><i>Chapter 3 – Research Intended .....</i></b>	<b>30</b>
<b>3.1 – Mono-objective Bio-based UP Synthesis Optimisation .....</b>	<b>30</b>
<b>3.2 – Mono-objective Bio-based RD Synthesis Optimisation.....</b>	<b>32</b>
<b>3.3 – Multi-objective Bio-based UPR Thermoset Curing Optimisation .....</b>	<b>33</b>
<b><i>4.0 – Appendix .....</i></b>	<b>34</b>
<b>4.1 – Preliminary Experimental Work Appendix .....</b>	<b>34</b>
<b>4.2 – BBAPT Optimisation Problem Framing Appendix .....</b>	<b>37</b>
<b>4.3 – P(GCiIt) System Optimisation Appendix.....</b>	<b>38</b>
<b><i>5.0 – Acknowledgements .....</i></b>	<b>42</b>
<b><i>6.0 – Bibliography .....</i></b>	<b>42</b>

## Acronyms & Abbreviations

Abbreviation	Meaning
B.....	Bio-based
BBAPT.....	Biodegradable bio-based aliphatic polyester thermoset
BO.....	Bayesian optimisation
Ci.....	Citric acid
C.....	Conventional
DoE.....	Design of experiment
D8.....	Eight sample prior-initialising dataset
D16.....	Sixteen sample prior-initialising dataset
EI.....	Expected improvement
G.....	Glycerol
GFRP.....	Glass fibre reinforced plastic
GP.....	Gaussian process
Gr.....	Grid
It.....	Itaconic acid
PB.....	Partially bio-based
PI.....	Probability of improvement
PR.....	Pseudorandom
P(GCi).....	Poly(glycerol citrate)
P(GCiIt).....	Poly(glycerol citrate itaconate)
P(GCiItSu).....	Poly(glycerol citrate itaconate succinate)
P(GIt).....	Poly(glycerol itaconate)
QR.....	Quasirandom
RD.....	Reactive Diluent
SDG.....	Sustainable development goal
SF.....	Space-filling
Su.....	Succinic acid
UP.....	Unsaturated polyester
UPR.....	Unsaturated polyester resin
UN.....	United Nations

## Symbols

Symbol	Typical Meaning
$x, y, z.....$	Scalars are lowercase
$\mathbf{x}, \mathbf{y}, \mathbf{z}.....$	Vectors are bold lowercase
$\mathbf{X}, \mathbf{Y}, \mathbf{Z}.....$	Matrices are bold uppercase
$\mathbf{X} = [\mathbf{x}_1, \mathbf{x}_2, \mathbf{x}_3] .....$	Matrix of column vectors stacked horizontally
$\mathbb{R} .....$	Real Numbers
$\mathbb{R}^d .....$	$d$ -dimensional vector space of real numbers
$\Delta .....$	Change
$a \in A .....$	$a$ is an element of the set $A$
$ \cdot  .....$	Absolute value
$P(H E) .....$	Probability of $H$ conditioned on $E$
$[l, h] .....$	Real numbers between $l$ and $h$
$Q \sim p .....$	Random variable $Q$ distributed according to $p$
$Ber(\mu) .....$	Bernoulli distribution with parameter $\mu$

# Chapter 1 – Rationale & Literature Review

The global chemical sector was estimated to be responsible for 5.8% of the 49.4 Mt CO<sub>2</sub>-eq of greenhouse gas (GHG) emissions released in 2016 (1, 2), these GHGs are responsible for anthropogenic climate change. Plastic manufacture is a growing industry within this sector, with the quantity of virgin material produced having grown from 329 Mt yr<sup>-1</sup> in 2013 (3) to 460 Mt yr<sup>-1</sup> as of 2019 (4). Resultant polymeric materials can be thermoplastic or thermosetting, the former remoulds on heating whilst the latter exhibits irreversible curing caused by chemical cross-linking between polymer chains (5). Given that ~184 Mt yr<sup>-1</sup> thermoplastic and ~8 Mt yr<sup>-1</sup> thermoset waste were generated in 2022 (6), the published literature is predominantly focused upon thermoplastic wastes and their associated breakdown productions, including microplastics (7-9). Despite being less prevalent, thermoset waste still presents a unique challenge worth addressing: the covalently cross-linked structure which previously afforded these materials their characteristic stiffness/strength also imbued an extreme resistance to biodegradation and recycling (10). Energy intensive procedures are therefore used to recycle these materials (11), which may therewith indirectly spur further demand for fossil fuels. This challenge is addressed in the 1<sup>st</sup> year's work of this PhD, where the optimisation problem of designing a strong yet biodegradable thermoset material is considered.

Aside from the GHG emissions incurred directly (fossil fuel burnt to provide energy for processes) and indirectly (GHGs produced as by-products of processes) by the chemical industry (2), a third emissions route via waste streams exists. Virtually all monomers which go into the manufacture of the estimated 30 Mt yr<sup>-1</sup> (2013, excl. elastomers and polyurethane) thermoset material are derived from fossil fuel feedstocks (3), which, on degrading can release fossil carbon trapped in polymeric matrices to the environment. Traditionally, a fibreglass composite material that contains a polyester thermoset matrix would be incinerated as part of an energy recovery process, therewith releasing fossil carbon to the atmospheric reservoir as CO<sub>2</sub> (12, 13). Alternatively, an inert thermoset material derived from bio-based feedstocks could provide either a net neutral impact on the atmospheric carbon reservoir if combusted, and a net negative impact if correctly stored in a pedospheric/geospheric reservoir. Work envisaged beyond the 1<sup>st</sup> year would entail the optimisation of desirable properties in novel bio-based thermosets composites.

## 1.1 – Literature Review

In 1987, the concept of ‘sustainable development’ was defined by the United Nations (UN) Brundtland Commission as a development which seeks to “meet the needs and aspirations of the present without compromising the ability to meet those of the future” (14). Wind turbine manufacturing is an industry shaped by this ideal, with its end-products contributing towards the UN’s 13<sup>th</sup> sustainable development goal (SDG) which urges “urgent action to combat climate change and its impacts” (15). Unfortunately, wind turbine blades are commonly manufactured from a composite comprised of thermosetting polymer matrix and reinforcing material, these strong thermoset matrices are chemically cross-linked which makes them difficult to reprocess or remould (16). Given this resistance to recycling and a relatively common rate of replacement (circa once every fifteen years in China (13)) this industry generates a large volume of practically unrecyclable thermoset waste which contravenes the UN’s 12<sup>th</sup> SDG to “ensure sustainable consumption and production” (15). In addressing the industry’s sustainability shortfall identified above, the literature can be mainly characterised by two different approaches. Firstly, there are papers which focus upon improving the recycling of the contemporary materials, whether by thermal, chemical, mechanical, or high-voltage fragmentation methods (17-19). Secondly, there are papers aimed at the development of

properties in future replacement materials that would facilitate recycling (20), such as introduction of chemically cleavable bonds into the thermoset polymers used (21). This report and the 1<sup>st</sup> year of research presented herein aligns with the latter set of papers.

Composites such as those found in wind turbine blades use a specific form of thermoset called a moulding thermoset, three are produced: unsaturated polyester resins (UPRs), phenoplasts, and polyepoxides, which comprise 20%, 18%, and 6% of annual thermoset production, respectively (22). Given their relative market dominance, thermosets based on polyesters were focussed upon in the 1<sup>st</sup> year's work. Polyesters are a group of polymers susceptible to biodegradation, with aliphatic forms more so than aromatics (23). This biodegradation is considered two step, beginning with surface/bulk erosion or depolymerisation and ending with enzymatic hydrolysis (24); polyesters whose labile ester linkages undergo abiotic hydrolysis (i.e. without enzymatic action) are still termed biodegradable (25). Enzymatic hydrolysis has been reported in aliphatic chains with molecular weights as high as 56,000 g mol<sup>-1</sup> (26). Biodegradation of linear aliphatic polyesters formed from the condensation polymerisation of various diols and a diacids dominates literature (27-29), these form thermoplastics whose degradation is dominated by bulk erosion which causes a loss of 3D structure and non-linear deterioration of mechanical properties over time (30-32). Conversely, polyester thermosets are primarily degraded by surface erosion in the first instance (33), this provides greater linearity in loss of mechanical performance through time (34). Various degrees of crosslinking lead to different mechanical properties in aliphatic polyester thermosets (31). Poly(glycerol-co-sebacic acid) is an example of a thermosetting aliphatic polyester copolymer, where a condensation polymerisation mechanism is leveraged to react a triol (glycerol) with a diol (sebacic acid) (35). Given their biodegradable nature, ability to create cross-linked materials, and simplicity of synthesis, these polyesters were directly focused upon during the 1<sup>st</sup> year of research.

Another important factor when considering the UN's 12<sup>th</sup> SDG is that of a material's provenance (15) – if the underlying chemistry of a polymer is petrochemical in origin, then any carbon liberated from the material at end-of-life, whether by combustion for energy or biodegradation in landfill, will release fossil carbon from the long-term carbon cycle into the short-term carbon cycle that exists above the geospheric reservoir, contributing via an anthropogenic route towards global climate change. Materials whose carbon was entirely derived from reservoirs other than the fossil geospheric one would therefore be desirable – such materials are usually given the more general term bio-based, where the definition prescribed is as such: "an organic material in which carbon is derived from a renewable resource via biological processes" (36). This definition would encompass materials whose carbon is derived from recently photosynthetically fixed atmospheric carbon, which is a carbon reservoir besides the fossil geospheric one. Although bio-based biodegradable thermosetting polyester would fit the simple definition of a bioplastic: "a polymer which has been manufactured into a commercial product from a renewable resource" (37), the term will be avoided as bioplastics are more generally considered to come in three forms: bio-based & non-biodegradable, bio-based & biodegradable, and fossil-based & biodegradable (38). In summary, the specific family of polymers targeted in the 1<sup>st</sup> year of this PhD, were bio-based biodegradable aliphatic polyester thermosets (BBAP).

Given the potential of BBAPTs as sustainable replacements for conventional thermosets, research into possible formulations and methods of manufacture was undertaken in the 1<sup>st</sup> year of this PhD. Since a desirable BBAPT would have greater biodegradability and similar strength to conventional thermosets, and these properties were a function of the formulation and manufacture of the material, an optimisation problem was foreseen. Optimisation is a technique which aims to find values for a set of variables which optimize a multivariate function given constraints on a search space (39). Optimisation can take place within a 'Design of

Experiments' (DoE) framework, a methodology for the development of a statistical model for the system response in which the input variables (factors) are modified and output variables (responses) are measured in a designed manner (40). DoE is commonly used for optimisation of a process; multifactor DoE (e.g. two-level factorial DoE), where multiple variables are varied simultaneously between experiments, is considered a more sample-efficient optimisation method when compared with traditional one-factor-at-a-time techniques (41). Multifactor DoEs are applied in two steps within an overarching procedure, initially a screening design is used to identify dominant factors whereafter an optimisation design (e.g. response surface method) is used to generate a final comprehensive model of the response surface and facilitate optima identification (42). In the response surface method optimisation design, a central composite factorial experiment is initially used to sample over the dominant factors' ranges, whereafter second order polynomials are fitted and gradient descent used to iteratively converge on an optimal point, this is a form of sequential design (43). Sequential sampling is favoured over one-shot methods as they avoid immediate imposition of a sample size and distribution across the factors' ranges (a.k.a. parameter/design space) at the start of an experiment based on limited prior knowledge of the target function – this being achieved by selecting points to sample based on previous iterations (44). Sequential sampling designs which adapt to features discovered within the parameter space during an iterative optimisation routine can be termed adaptive sampling (45) or adaptive experimental designs, these have been used to enhance sample efficiency of optimisation designs (46). Given their potential to accelerate discovery of materials with sustainable properties, these sequential (adaptive) techniques were considered further within the BBAPT scope of this 1<sup>st</sup> year of research.

An example of a BBAPT would be poly(glycerol citrate), which is formed via the condensation polymerisation of the triol glycerol and triacid citric acid (47). Despite apparent simplicity of this two reactant system, polycondensation is dependent upon multiple variables: temperature, stoichiometric ratios, and additive presence (48). These affect final 3D structure of the thermoset material, subsequently affecting biodegradability and mechanical properties. Given this, a function linking a continuous objective metric (e.g.  $y$  as tensile strength) of a material's performance with a high number of input variables (e.g.  $x_1, x_2, x_3$  as curing temperature, stoichiometry, filler content) relating to its composition/manufacture can be postulated (Eq. 1). This function is black-box given its opacity with respect to inner-workings and lack of derivatives (49), and would be more generally described in arrow notation in Eq. 2 and elementarily in functional form in Eq. 3.

$$y = f(x_1, x_2, x_3) \quad \text{Eq. 1}$$

$$f: \mathbb{R}^n \rightarrow \mathbb{R} \quad \text{Eq. 2}$$

$$f(\mathbf{x}) \text{ where } \mathbf{x} = (x_n, x_{n+1}, \dots) \quad \text{Eq. 3}$$

In the case of poly(glycerol citrate) feedstocks are low-cost but reaction times for rigid solid thermoset materials are on the order of weeks when uncatalyzed (50); catalysis commonly involves strong fuming acids which corrode equipment and are best avoided (51). Given that an evaluation of a function such as Eq. 1 for poly(glycerol citrate) takes around 7 days, only around 52 data points could be generated in a sequential optimisation process over the period of a year. This temporal limitation on sampling makes evaluations of the poly(glycerol citrate) system's function relatively expensive in nature. Given the high dimensionality, black-box nature, and temporal expense of function evaluation a sequential optimisation technique known as Bayesian optimisation (BO) was identified as lending itself well to the accelerated development of desirable properties in BBAPTs. Alternative global optimisation techniques were considered but ruled out; the hill-climbing class gradient descent algorithm was reliant on derivatives of the objective function (52), which would have been uncertain and practically difficult to obtain given the noisy real-world nature of the black-box function evaluated. The population class evolutionary and particle swarm optimisation algorithms were suitable but avoided in favour of the more sample efficient surrogate class of algorithms. Surrogate class algorithms are variously formulated, but the three major forms are distinguished by the surrogate models they leverage- polynomial response surface model (RSM), kriging (aka gaussian process regression), radial basis function (RBF) (53). Kriging is preferable to RSM since it makes no assumption of polynomial order, avoiding *a priori* bias in surrogate models generated. Meanwhile RBF-based surrogate models provide no estimates of uncertainty around the fitted function; functions and associated uncertainties derived using kriging provides the means by which BO effectively balance exploitation and exploration of the parameter space. The 1<sup>st</sup> year of research revolved around the development of a part-computational and part-laboratory based workflow for optimisation of properties in BBAPTs leveraging BO predicated on kriging (54).

Originally coined in the 1970s by Mockus *et al.* (55), Bayesian optimisation was later developed further in the 1990s by Jones *et al.* into a technique called the efficient global optimisation algorithm (56) – this name and technique was thereafter adopted and popularised by the DoE community. More recently, the original name has seen a revival as the technique and a plethora of adaptations have been re-discovered and implemented in a range of contemporary communities including robotics (57), bioengineering (58), and machine learning (59). In materials science, BO has been used to predict crystalline structures (60), carry out sample-efficient optimisation of density functional theory simulations (61), and multi-objective optimisation of stability and ion-conductivity in materials (62).

## 1.2 – Report Overview

Having introduced the project and reviewed relevant literature in Chapter 1, this report moves onto “Chapter 2 – Research Completed”. This Chapter guides the reader through experimental, mathematical, and computational method developed and applied during the 1<sup>st</sup> year of research. Initially, Chapter 2.1 describes the basic experimental methods motivating the project and how these guided which parameters were to be considered for the optimisations. Based on this, Chapter 2.2 provides a detailed discussion of how the optimisations were framed mathematically, by showing how constraints were imposed and random sampling carried out. Following this, Chapter 2.3 returns to experimental method by describing how materials were manufactured and characterised after parameterisation. Subsequently, Chapter 2.4 provides background on behaviour of the sequential sampling procedures programmed as well as describing what specific methods were applied. Finally, Chapter 2.5 presents a comparison of benchmark and Bayesian optimisations for a specific chemical system, the results are visualised and described before a discussion is provided. In “Chapter 3 – Research Intended” a plan for the next two years of research is detailed and the initial set of challenges expected discussed.



## Chapter 2 – Research Completed

At the start of the 1<sup>st</sup> year, a simple hypothesis was posited; “Bayesian optimisation can be used to increase the sample efficiency when optimising the properties of BBAPTs”. Initially, a poly(glycerol citrate) thermoset (P(GCi)) was selected as a suitable polyester thermoset on whose chemistry a BO workflow could be developed. Naturally it follows that if a proof-of-concept workflow could be developed to successfully optimise the model P(GCi) system, the initial hypothesis could be supported whilst assembling the codebase and experimental techniques necessary for optimisation of more complicated chemical systems later in the PhD.

Before BO of a BBAPT can take place, a desired dependent variable (target variable) must be identified, and a set of controllable dependent variables (predictor variables) elected. These are indispensable during BO as the optimiser attempts to find the best combination of values for the predictor variables generating the best target variable value. In Chapter 2.1, we describe how the target variable of mass loss is selected based on the polymer chemistry of the P(GCi) BBAPT, before concluding that stoichiometry of reactants likely has the greatest impact on the target variable and should therefore be parameterised by any eventual predictor variables selected.

In Chapter 2.2, predictor variables are conceived of which link mathematically to stoichiometry of reactants, which in turn link experimentally with the finally evaluated target variables. This finally describes a BBAPT BO problem fully: If stoichiometries are dependent upon predictor variables and can be directly calculated, and target variables are dependent upon stoichiometries and are mapped via an unknown function, then target variables are effectively dependent upon predictor variables via an unknown function. BO is the optimisation of this unknown black-box function by applying Bayesian methods, in effect, a sequential sampling technique where information previously known about the black-box’s functional link is used to strategically select combinations of values for predictor variables which are likely to yield improved values for the target variable. Given BO’s reliance upon previous information, some form of initial information must be provided- this is the prior-initialising dataset, a sparse but representative matrix of predictor variable combinations and target variable values. Here, representative refers to the predictor variable combinations being well-spread across the entire region of possible combinations (a.k.a. parameter space), such combinations are usually initially obtained using deterministic space-filling sampling techniques. Chapter 2.2 will therefore also describe how these space-filling techniques were tailored to produce representative matrices of predictor variable combinations.

How a specific combination of predictor variables’ values (and thereby stoichiometric ratios) is used to inform experimental preparation of a BBAPT sample and its subsequent characterisation in terms of the target variable value is described in Chapter 2.3. This is effectively a description of the computationally-automated and experimentally implemented process by which the black-box function is evaluated.

Once the black-box function evaluation method has been applied to all the combinations provided by an initial space-filling sampling technique, and all the target values have been obtained, a full prior-initialising matrix will have been created- this dataset allows the sequential sampling procedure to begin. How BO (Bayesian sequential sampling) uses this prior-initialising dataset to strategically sample the parameter space is presented in Chapter 2.4 where it begins by describing how Bayesian optimisation routines consist of a Bayesian statistical model and an acquisition function. The Bayesian statistical model which is fit to the data as a surrogate model (a function mimicking the behaviour of another) of the objective function, is a Gaussian process describing the expected mean target value and its covariance for any given combination of predictor variable values. Meanwhile the acquisition function is one informed by the Gaussian process and which takes combinations of predictor variable

values and returns a metric such as probability of improvement (upon best combination of predictors and associated target discovered so far). This acquisition function can then be cheaply optimised using an off-the-shelf optimiser to find the combination of predictor variables' values with the highest probability of improvement- this combination is thereafter provided by the BO routine as the strategically best point to sample next within the parameter space. Additionally, Chapter 2.4 notes the specific assumptions and techniques applied.

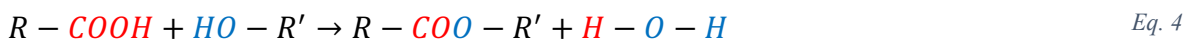
Finally, all the above methods are brought together in Chapter 2.5 where numerous differently parameterised optimisations are set up to gauge the capability of the Bayesian sequential optimisation technique relative to the classical deterministic space-filling techniques. This chapter begins by introducing the specific BBAPT system to be optimised and contextualising eventual results by presenting the theoretical maximum target values. Subsequently, the benchmark deterministic space-filling optimisation techniques are described, and their results tabulated, before the same is done for the Bayesian sequential optimisations. Following this, a comparison of the various space-filling and sequential trials are presented as progressions, with the best target values found at a given iteration plotted against number of samples taken. Thereafter, further analysis of results is carried out and discussion regarding observations of interest provided before conclusions are reached regarding the initially postulated project hypothesis.

## 2.1 – Preliminary Experimental Work

Before BO of a BBAPT could be carried out, experimental technique for the manufacture of these polymers had to be explored – this provided insights into the metric by which success could be gauged in an eventual optimisation (target variables) as well as the key variables influencing these metrics of interest (predictor variables). These are key to a BO routine as they provide a target variable to be maximised and the associated predictor variables to be optimised. This section starts by detailing how a suitable target variable was identified, before identifying the dominant variable affecting this target.

### 2.1.1 – Target Variable Identification

To start with, an experimental method was replicated and adapted from a previous paper by Alberts *et al.* (48). In that paper, varying ratios of glycerol and citric acid (Figure 1) were mixed in a beaker using a hotplate stirrer to agitate the mixture whilst heating it to 130 °C. This was carried out until all solid acid had visibly dissolved into the glycerol. A concentrated sulphuric acid catalyst was thereafter added before the mixture was placed in a drying oven for various time periods (from hour to day scale). Once homogenous, a sample of the liquid was transferred to a silicone cube mould and placed in a drying oven to bake (day to week scale) until a thermoset developed from the polycondensation polymerisation reactions described below.



The condensation reaction occurring between carboxyl and hydroxyl groups is an esterification reaction, which in simple terms occurs via the reaction described in Eq. 4 and Eq. 5. It is described as a condensation reaction since a small by-product molecule, water, is generated as each ester bond is formed. Note, for the sake of brevity the entire five step esterification reaction mechanism is not drawn here. Given the chemicals of interest in the Alberts *et al.* (48) paper, the esterification is likely to take place between any of the carboxyl groups on triacid or diacid molecules, and any of the hydroxyl groups located on the triol molecule (Figure 1).

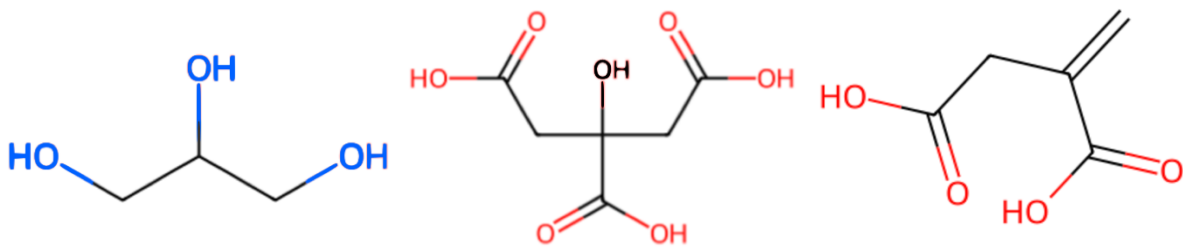


Figure 1 – Skeletal diagrams of chemicals studied. Left: Glycerol. Centre: Citric acid. Right: Itaconic acid. Functional groups considered likely to be taking part in the esterification are coloured: Blue for hydroxyl groups, Red for carboxyl groups.

Since these esterification reactions take place between multi-functional molecules in Alberts *et al.* (48), polyesterification can occur. Polyesterification is a form of polycondensation reaction which takes place as follows: an initial ester is formed from two difunctional monomers, where one must at least be a diol and the other a diacid (or both having both a carboxyl and a hydroxyl group), producing a molecule of water and an ester with two spare functional groups- these groups can subsequently react with more difunctional monomers causing polymerisation into a linear polyester. When monomers with a functionality greater than two are introduced into a polyesterification reaction, then side chains can form along the primary backbone of the growing polyester, this causes the development of a branching polymeric structure. When a side chain reaches another large growing polyester molecule and reacts with it a crosslink is said to have developed; when widespread crosslinking occurs generating a 3D network of polyester molecules a thermoset polyester has been created. In Figure 2 an example of a branching structure developing out of the reaction between glycerol (triol) and citric acid (triacid) is presented.

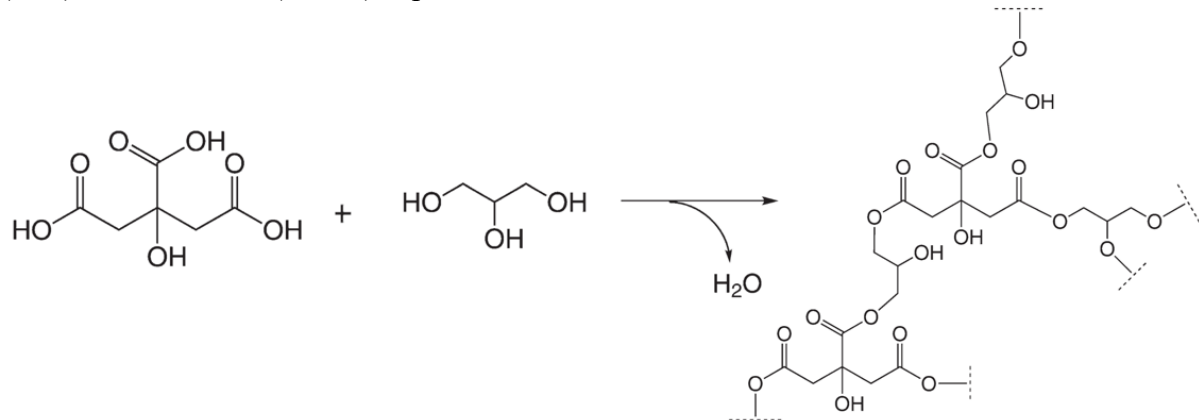


Figure 2 – Skeletal diagram presenting the polycondensation reaction between a triol (glycerol) and a triacid (citric acid). Adapted from (47).

In our adapted method, a hotplate temperature of 140 °C was adopted to accelerate the dissolution without encouraging decarboxylation of the citric acid to itaconic acid which is known to take place at temperatures exceeding 150 °C (48). Furthermore, the catalyst was omitted as the drying ovens would be corrosively damaged by fuming sulphuric acid vapours; it seemed this would slow but fail to halt polycondensation (63). Since the polycondensation which proceeds between the triol and triacid is a simple esterification reaction which generates water as the only by-product, mass loss between the start and end of the experiment (predominantly comprised of evaporating water) can be considered a proxy for extent of polymerisation within the thermoset (50). This mass loss  $\Delta m$  was calculated as the difference in mass between the prepolymer mass  $m_p$  (i.e. mass of reactants) and the final thermoset mass  $m_t$  (i.e. mass of final solid) (Eq. 6) and is later used in a percentage format  $\Delta m\%$  (Eq. 7).

$$\Delta m = m_p - m_t \quad Eq. 6$$

$$\Delta m\% = \frac{\Delta m \times 100}{m_p} = \frac{(m_p - m_t) \times 100}{m_p} \quad Eq. 7$$

Since masses were measured using a mass balance accurate to  $0.01\text{ g} \pm 0.01\text{ g}$ , the samples were  $3.00\text{ g}$  in mass and  $\Delta m$  was expected to be between  $0.30\text{-}0.90\text{ g}$  (See Chapter 2.5.1) systematic errors accrued through uncertainty in mass balance readings were considered negligible. Percentage mass loss  $\Delta m\%$  was therefore selected as the target (objective/response/dependent) variable for the BBAPT optimisation experiments.

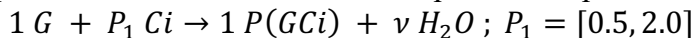
### 2.1.2 – Constant & Predictor Variable Identification

An early issue encountered with the adapted method was premature polymerisation of glycerol and citric acid during the dissolution process, causing vigorous bubbling (water vapour) which precluded visual inspection for completion of dissolution. This led to the adoption in preliminary experimentation of itaconic acid (Figure 1) over citric acid, which was known to generate thermoset materials, yet did not suffer from the same drawback (48). Once several poly(glycerol itaconate) (P(GIt)) samples had been successfully prepared using the adapted method with arbitrary stoichiometries and drying oven temperatures, it was found that samples exhibited varying degrees of foaming, which was a natural consequence of water vapour entrapment within the solidifying matrix. Based on these tests it was hypothesised that foaming would introduce a confounding factor which would obfuscate the effect of other variables upon the mass loss target variable, and that drying oven temperature had the greatest effect upon degree of foaming. To investigate this further a screening design experiment was conducted wherein drying oven temperatures and stoichiometric ratios (glycerol : itaconic acid) were varied in a controlled manner and mass loss measured. After visual inspection of the samples it was concluded that higher concentrations of itaconic acid and higher drying oven temperatures led to higher degrees of foaming, with practically all foaming mitigated at temperatures below  $90\text{ }^{\circ}\text{C}$  (A1, A2). This generated a working hypothesis that water generated below  $100\text{ }^{\circ}\text{C}$  was failing to vaporise and hence remaining in a liquid state, this liquid water could therefore remain homogenous within the prepolymer since hydrogen bonding could occur between glycerol's alcohol groups and water- aptly explaining reduced foaming at higher concentrations of glycerol and lower temperatures. Further to this, data was analysed for each of the temperatures tested (A3-A7) by plotting the mass loss against normalised itaconic acid concentration and fitting a Gaussian process surrogate model to these, providing a mean function and inferential uncertainty (visualised by the 95% credible interval). As the temperatures reduced the underlying function changed to show a clear trend between low itaconic acid concentration and high mass loss, whilst the inferential uncertainty reduced around the mean function- this shows that by reducing the temperature (and therewith the foaming) a factor which was obfuscating the functional link between stoichiometry and mass loss was removed. It was therefore decided that all future experiments on BBAPTs would adopt a constant variable for drying oven temperature of  $90\text{ }^{\circ}\text{C}$ . After formalisation of the basic experimental procedure and control of confounding variables, stoichiometry was selected as the basis for predictor (factor/explanatory/independent) variables in the BBAPT optimisation experiments.

## 2.2 – Optimisation Problem Framing

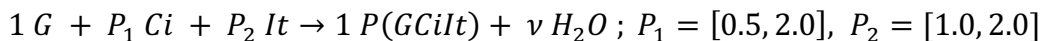
Having selected percentage mass loss  $\Delta m\%$  as the target variable for the optimisation of a given BBAPT, the associated predictor variables to be optimised had to be conceived of. In principle, these predictor variables would inform the stoichiometric ratios of chemicals used in the manufacture of a BBAPT sample, and thereby the target values obtained for that sample upon characterisation. By describing the direct mathematical link between predictor variables and stoichiometries, and assuming the unknown mapping between these stoichiometric ratios and the characterised target variable values, a black-box optimisation task is fully described.

In this section multiple different BBAPT “chemical systems” are described; these are simply stoichiometric equations describing the reaction between a single mole of glycerol and any number of organic acids (specifically di/tri-acids). A simple BBAPT chemical system is seen in Eq. 8, where one mole of glycerol  $G$  reacts with an unknown number of moles of citric acid  $Ci$  to produce a mole of poly(glycerol citrate)  $P(GCi)$  and an unknown number of moles of water  $\nu$ . Here, a stoichiometric predictor variable  $P_1$  could simply be the number of moles of citric acid. Informed by the functionality of citric acid relative to glycerol (i.e. ratio of carboxyl groups to hydroxyl groups), a constraint in the form of upper and lower bounds can be placed on this stoichiometric predictor variable ( $P_1 = [0.5, 2.0]$ ) to ensure that a random predictor variable drawn from the parameter space could never fail to polymerise.



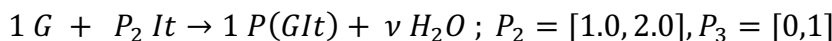
*Eq. 8*

A more complex BBAPT system is presented in Eq. 9. If moles of citric and itaconic acid ( $It$ ) are simply set as stoichiometric predictor variables  $P_1, P_2$  with upper and lower constraints ( $P_1 = [0.5, 2.0]$ ,  $P_2 = [1.0, 2.0]$ ), then the parameter space is not well-constrained enough. For example, no random combination of predictor variables allowed for one acid to fall to zero allowing complete dominance of another acid. And if this were solved by changing the constraints to ( $P_1 = [0.0, 2.0]$ ,  $P_2 = [0.0, 2.0]$ ), then there would always be a chance that a randomly drawn sample could be  $P_1 = 0, P_2 = 0$  where no polymerisation would be successful and no target value could be evaluated.



*Eq. 9*

To tackle this, complicated BBAPT chemical systems were broken back down into simple chemical systems termed “acid systems”. Separate acid systems for citric and itaconic acid are presented in Eq. 10 and Eq. 11 respectively. These acid systems could have their molar values constrained in the same way as for the single acid system (using the stoichiometric predictor variables  $P_1, P_2$ ), before a ‘balancing’ predictor variable  $P_3$  could be used to modify the stoichiometric predictor variable and thereby assert dominance of one acid system over another. This was asserted by multiplication of balancing predictor with stoichiometric predictor:  $P_1 \times P_3$  and  $P_2 \times (1 - P_3)$ . This allowed the entire parameter space to be explored, since a randomly sampled combination of predictor variable values could never fail to polymerise whilst one acid could in some cases dominate entirely over the other.



*Eq. 10*

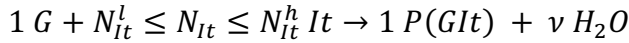
*Eq. 11*

Since the balancing variable now modified the stoichiometric predictor variables to create new stoichiometric predictor variables, it was decided that the initial variables be normalised and renamed to ‘strength’ predictor variables with symbol  $s$ , whilst the modified values retained the name of stoichiometric variables with symbol  $N$  given that these were the actual stoichiometries used during experimental preparation of samples. Balancing predictor variables were accordingly given the symbol  $b$ .

Chapter 2.2 presents a series of BBAPT chemical systems of monotonically increasing complexity and shows how strength and balancing predictor variables are parameterised for each. Furthermore, the equations linking these predictor variables to stoichiometric variables are shown- this links a given combination of predictor variables’ values to stoichiometric variables’ values, which subsequently link to the target variable value via experimental implementation of sample manufacture and characterisation (See Chapter 2.3). Additionally, Chapter 2.2 provides the method by which representative random sampling of predictor variables’ values can be carried out using space-filling sampling techniques.

### 2.2.1 – 1D Optimisation Problem for P(GIt)

Given the poly(glycerol itaconate) (P(GIt)) BBAPT chemical system, a stoichiometric equation could be written as seen in Eq. 12. Lower  $N_{It}^l$  and upper  $N_{It}^h$  constraints can be placed on the stoichiometric variable  $N_{It}$  dictating moles of itaconic acid relative to the constant 1 mole of glycerol.



Eq. 12

When the functionality of the two reactants involved in this reaction are considered, a series of illustrations describing potential bonding at different molar ratios can be drawn (Figure 3). From this illustration, an approximate range of ratios that can generate polymerizable repeat units can be deduced, providing the lower ( $N_{It}^l = 1$ ) and upper ( $N_{It}^h = 2$ ) constraint values for the stoichiometric variable.

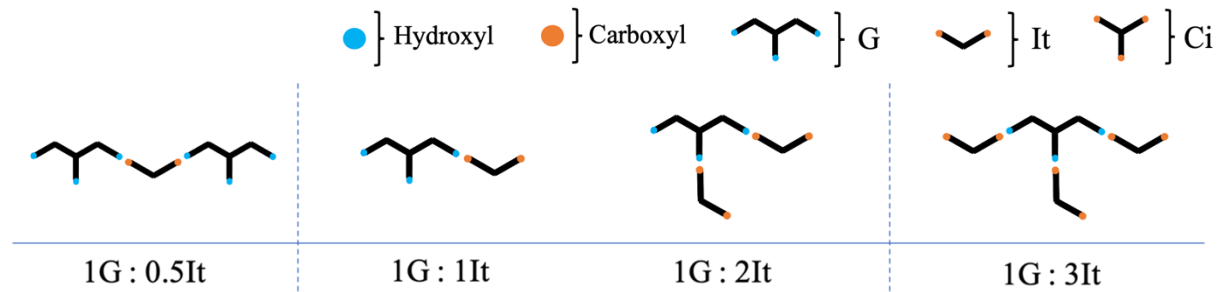


Figure 3 – Illustration of stoichiometric ratios between glycerol (G) and itaconic acid (It) and possible repeat units.

This optimisation problem is considered one dimensional (1D), as only one dimension (predictor variable) is required to describe the parameter space of the sole stoichiometry variable that exists in the chemical system.

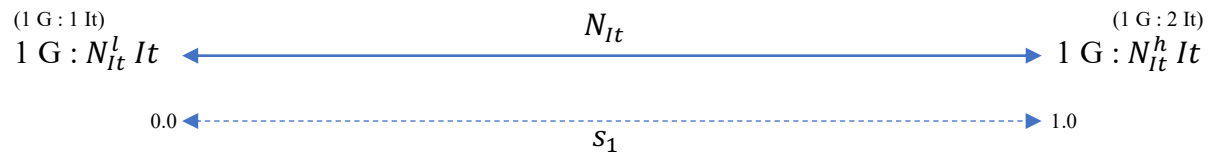


Figure 4 – Visualisation of 1D optimisation parameter space for the P(GIt) problem.

The relationship between the single stoichiometry variable and the single strength predictor variable  $s_1$  needed to describe it is visualised in Figure 4, and the equation describing the conversion is shown in Eq. 13.

$$N_{It} = N_{It}^l + (N_{It}^h - N_{It}^l) * s_1$$

Eq. 13

At this point the Bayesian optimisation task can be expressed as the maximisation of a black-box function ( $f$ , Eq. 14) where the global optimum for a predictor variable's value ( $\mathbf{x}^*$ , Eq. 15) is the end goal of the sequential optimisation process, each query of the function takes a different predictor variable value ( $\mathbf{x}$ ) from the bounded domain (a.k.a. parameter space,  $A$ ) and returns a target value ( $\Delta m \% \subseteq \mathbb{R}$ ) which is a percentage mass loss value. The absolute percentage mass loss indicates the % loss of mass between the start mass of prepolymer (combined mass of reactants) and the end mass of thermoset after being exposed to the drying oven, this controls for different masses of prepolymer being added to the moulds. In the case of the 1D problem presented here, there is only a single predictor variable, strength predictor variable 1, but it will nonetheless be treated as if it were residing within an array of predictor variables since more complex problems detailed later will use this syntax (Eq. 14). Note that in Eq. 14 the  $i$  simply indicates which sample in a sequential sampling procedure is being considered,  $s_1^i$  therefore indicates the scalar value attributed to the strength predictor variable  $s_1$  of sample  $i$ .

$$\Delta m\% = f(\mathbf{x}) = f([s_1^i]) \quad \text{Eq. 14}$$

$$\mathbf{x}^* = \arg \max_{\mathbf{x} \in A} f(\mathbf{x}) \text{ where } f: A \rightarrow \mathbb{R} \text{ and } A \subseteq \mathbb{R}^d \quad \text{Eq. 15}$$

Before sequential optimisation can begin, representative sampling of the parameter space must be carried out to generate a balanced dataset ( $\mathbb{D}$ , Eq. 17) which can be used to create a fair overview of the parameter space. This dataset (matrix) is comprised of all the combinations of predictor variable values trialled thus far ( $\mathbf{X}$ , Eq. 16) and all the target values yielded from function evaluations using these combinations ( $f(\mathbf{X})$  or  $\Delta m\%$ ).

$$\mathbf{X} = [\mathbf{x}^{i=1}, \mathbf{x}^{i=2}, \dots] = [[s_1^{i=1}], [s_1^{i=2}], \dots] \quad \text{Eq. 16}$$

$$\mathbb{D} = [\mathbf{X}, f(\mathbf{X})] = [[\mathbf{x}^{i=1}, \mathbf{x}^{i=2}, \dots], [f(\mathbf{x}^{i=1}), f(\mathbf{x}^{i=2}), \dots]] \quad \text{Eq. 17}$$

Initial space-filling sampling in the continuous parameter space can be carried out in one of three ways: grid, pseudorandom, or quasirandom (Figure 5). Grid sampling discretises each of the predictor variables ranges and generates an exhaustive combinatorial search of the parameter space, this is highly representative but fails to scale to higher dimensions in a sample efficient manner. Pseudorandom sampling uses pseudorandom number generation (computationally derived) to draw samples from a continuous uniform distribution across the parameter space, this scales to higher dimensions but fails to guarantee representative sampling of the space (64). Quasi-random sampling suffers from neither of these two issues and is generally considered the most suitable for Bayesian optimisation problems that require sample-efficiency and representative priors. Sobol sampling was selected as the quasirandom techniques used in this work as it has been found to provide the same or better space-filling properties across  $\mathbb{R}^{1 \leq n \leq 40}$  domains (45). This sampler was programmed in python (version 3.10.10) and drew on libraries including Pandas (65), NumPy (66), SciPy (67), and Matplotlib (68).

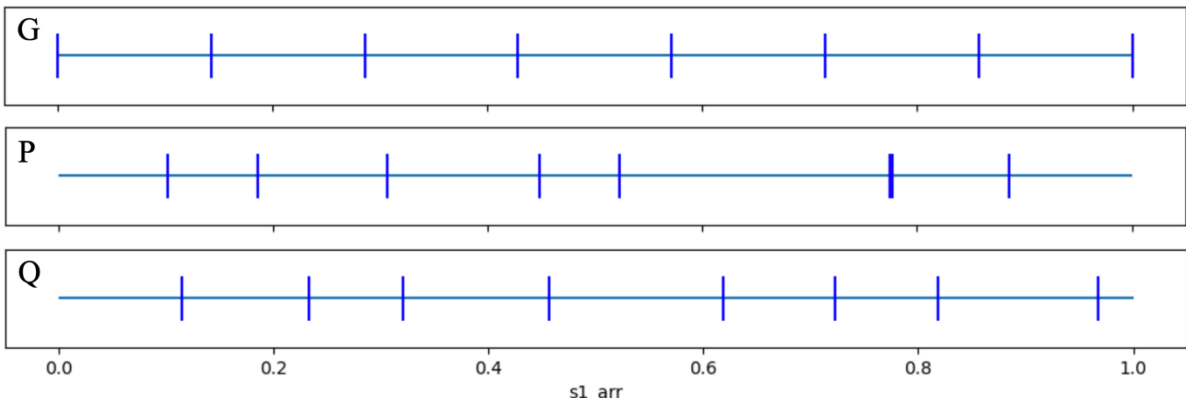


Figure 5 – Visualisation of 27 predictor samples taken from the strength predictor variable's ( $s_1$ ) range: these are distributed in a gridded (G), pseudorandom (P), and quasirandom (Q) fashion across the 1D parameter space.

### 2.2.2 – 3D Optimisation Problem for P(GCiIt)

The optimisation of the P(GIt) system for the target variable  $\Delta m\%$  given only a singular strength predictor  $s_1$  was deemed trivial given the accuracy with which a small number of samples sampled across the parameter space characterised the entire functional link between the two variables (A7). Hence, as a more stringent test of methodology, the more complicated three-reactant chemical system based on glycerol, itaconic acid, and citric acid yielding the thermoset poly(glycerol citrate itaconate) (a.k.a. P(GCiIt)) was focused on. This system is presented in Eq. 18 with lower  $N_{Ci}^l$  and upper  $N_{Ci}^h$  limits for the citric acid stoichiometric variable  $N_{Ci}$  shown. Additionally, the acid systems are shown separately in Eq. 19 and Eq. 20.

$$1 G + N_{Ci}^l \leq N_{Ci} \leq N_{Ci}^h \quad Ci + N_{It}^l \leq N_{It} \leq N_{It}^h \quad It \rightarrow 1 P(GCiIt) + \nu H_2O \quad Eq. 18$$

$$1 G + N_{Ci}^l \leq N_{Ci} \leq N_{Ci}^h \quad Ci \rightarrow 1 P(GCiIt) + \nu H_2O \quad Eq. 19$$

$$1 G + N_{It}^l \leq N_{It} \leq N_{It}^h \quad It \rightarrow 1 P(GCiIt) + \nu H_2O \quad Eq. 20$$

The lower and upper constraints for the itaconic acid system are adopted from the previous 1D P(GIt) problem, whilst the citric acid stoichiometry variable  $N_{Ci}$  was constrained by a similar method using Figure 6, with lower ( $N_{Ci}^l = 0.5$ ) and upper ( $N_{Ci}^h = 2$ ) bounds set accordingly.

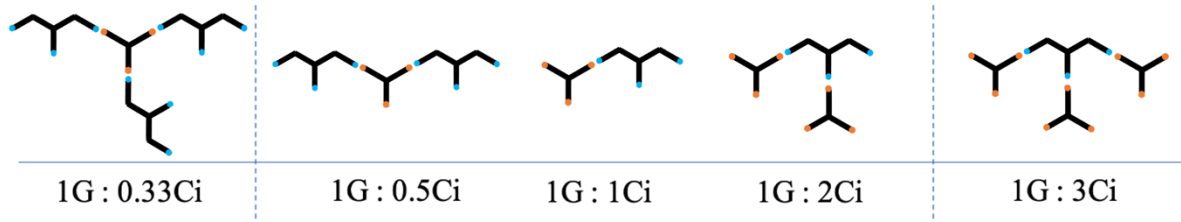


Figure 6 - Illustration of stoichiometric ratios between glycerol (G) and citric acid (Ci) and possible repeat units.

The P(GCiIt) system creates a 3D Bayesian optimisation problem, which requires a new visualisation to present the interplay between the predictor variables and stoichiometric variables (Figure 7). Now there are two strength predictor variables dictating the ratio of glycerol and the respective acid, whilst a third balancing predictor variable  $b_1$  balances the dominance of one acid system over another.

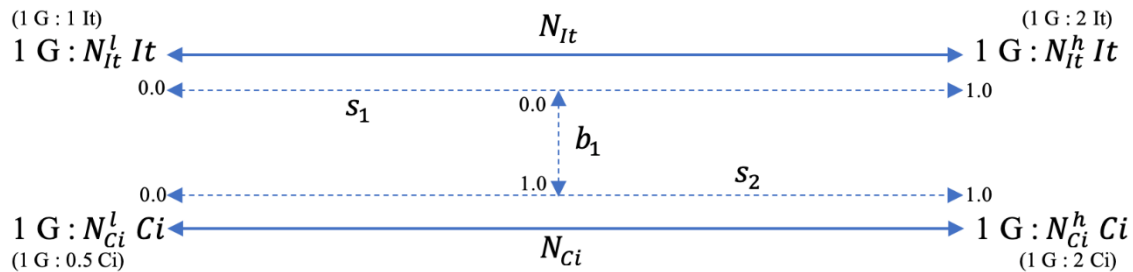


Figure 7 - Visualisation of 3D optimisation parameter space for the P(GCiIt) problem.

How the value of a stoichiometry variable is calculated from the strength predictor variable's value depends on whether citric acid ( $N_{Ci}$ , Eq. 22) or itaconic acid ( $N_{It}$ , Eq. 21) is considered. Stoichiometric variable values can thereafter be substituted into their respective positions within the modified overall stoichiometric equation for the chemical system in Eq. 23. When this modified equation is examined it becomes clear that the lower stoichiometric constraints set on acid systems have been broken and that they are in fact soft constraints, this is because balancing variables override these constraints; this is considered acceptable since the action of the balancing parameters always ensures that there is enough acid for polymerisation to take place and necessary because if lower bounds couldn't be broken then one acid system couldn't be entirely marginalised in favour of another during optimisation.

$$N_{It} = (N_{It}^l + (N_{It}^h - N_{It}^l) \times s_1) \times (1 - b_1) \quad Eq. 21$$

$$N_{Ci} = (N_{Ci}^l + (N_{Ci}^h - N_{Ci}^l) \times s_2) \times b_1 \quad Eq. 22$$

$$1 G + 0 \leq N_{Ci} \leq N_{Ci}^h \quad Ci + 0 \leq N_{It} \leq N_{It}^h \quad It \rightarrow 1 P(GCiIt) + \nu H_2O \quad Eq. 23$$

Given the well-constrained 3D parameter space above, the associated optimisation problem retains its goal of maximising the target variable value by finding the best possible combination of predictor variable values (Eq. 15), though the black-box function considered has become multivariate (Eq. 24). This is also reflected in the predictor variables' value matrix which grows as the optimisation proceeds (Eq. 25).

$$\Delta m\% = f(\mathbf{x}) = f([s_1^i, s_2^i, b_1^i]) \quad \text{Eq. 24}$$

$$\mathbf{X} = [\mathbf{x}^{i=1}, \mathbf{x}^{i=2}, \dots] = [[s_1^{i=1}, s_2^{i=1}, b_1^{i=1}], [s_1^{i=2}, s_2^{i=2}, b_1^{i=2}], \dots] \quad \text{Eq. 25}$$

In the optimisation practically carried out later in this report on the P(GCiIt) system, initial space-filling sampling was carried out using the Sobol quasirandom sampling technique across the three predictor variables described to generate a representative prior-initialising dataset.

### 2.2.3 – 5D+ Optimisation Problems for Complex BBAPT Systems

Although not tackled in the laboratory, higher dimensional problems were conceived of, and balancing mechanisms hypothesised. In the case of a 5D problem a custom sampler was programmed; this problem effectively incorporated succinic acid into the P(GCiIt) 3D problem to generate the more complicated poly(glycerol citrate itaconate succinate) BBAPT chemical system (Eq. 26). Since succinic acid is also a diacid, its stoichiometric constraints ( $N_{Su}^l = 1$ ,  $N_{Su}^h = 2$ ) were set equal to those of itaconic acid.

$$1G + 0 \leq N_{Ci} \leq N_{Ci}^h \quad Ci + 0 \leq N_{It} \leq N_{It}^h \quad It + 0 \leq N_{Su} \leq N_{Su}^h \quad Su \rightarrow P(GCiItSu) \quad \text{Eq. 26}$$

To frame this problem a third strength predictor variable  $s_3$  and a second balancing predictor variable  $b_2$  were introduced; how all the variables interlink with stoichiometric variables is seen in Figure 8. The two balancing predictor variables were confined to a 2D parameter subspace which took the form of a 2<sup>nd</sup> order simplex (equilateral triangle), in doing so, a ternary plot was created which allowed the ratio of the three acid systems to be calculated for any point defined by  $b_1$  and  $b_2$  within (application of the altitude method for ratios).

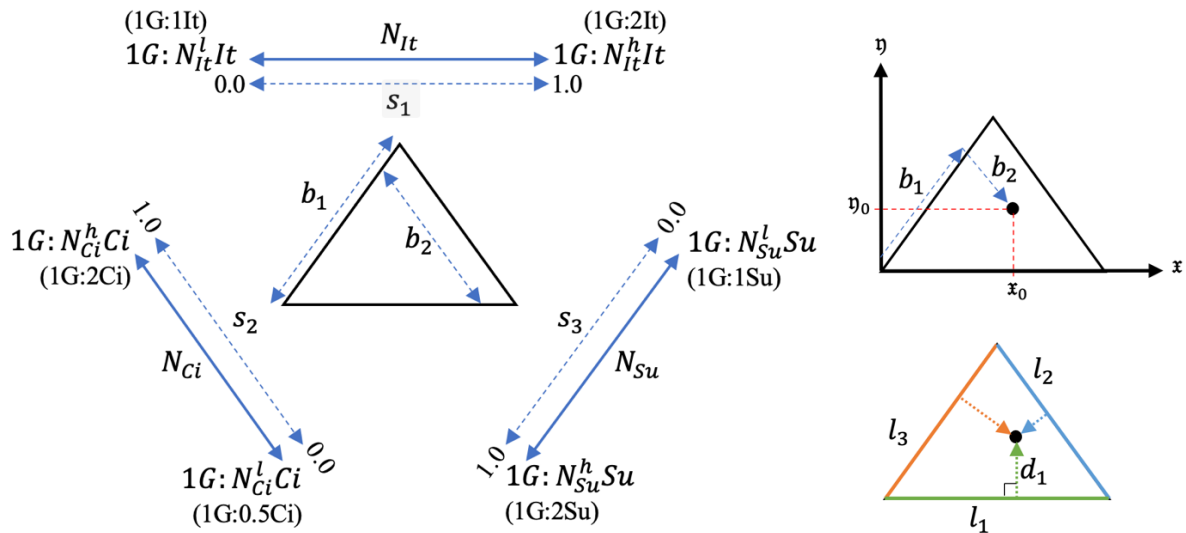


Figure 8 – Visualisation of 5D optimisation parameter space for the P(GCiItSu) problem. Left Hand Side, LHS: Overview diagram. Upper Right, UR: Translation of  $b_1, b_2$  coordinates to  $\mathfrak{x}, \mathfrak{y}$  coordinates. Lower Right, LR: Application of altitude method for ratio calculation.

Firstly, a point would be translated using the function  $f_t$  from  $b_1, b_2$  coordinates to the coordinates  $\mathfrak{x}_0, \mathfrak{y}_0$  of the Cartesian coordinate system defined by axes  $\mathfrak{x}, \mathfrak{y}$  (Eq. 27 & Figure 8UR). Secondly, the lines  $l_1, l_2, l_3$  (each associated with acid systems It, Ci, Su respectively) are defined as two variable linear equations with the associated constants ( $a, b, c$ ), this allowed distances between any line and a point to be calculated. For a given line (e.g.  $l_1$ ) the shortest distance (e.g.  $d_1$ ) to the point  $\mathfrak{x}_0, \mathfrak{y}_0$  could be calculated (Eq. 28 & Figure 8LR).

$$\mathfrak{x}_0, \mathfrak{y}_0 = f_t(b_1, b_2) \quad \text{Eq. 27}$$

$$d_1 = \frac{|a_1\mathfrak{x}_0 + b_1\mathfrak{y}_0 + c_1|}{\sqrt{a_1^2 + b_1^2}} \quad \text{Eq. 28}$$

Thirdly, by finding the relative length of a given line (e.g.  $d_1$ ) when compared with the combined length of all line lengths summed, a dominance variable of a specific acid system (e.g.  $h_{It}$ ) is obtained (Eq. 29). Finally, dominance variables evaluated can be used to calculate the stoichiometric variables for a specific acid system (Eq. 30), which can finally be substituted back into Eq. 26. The final 5D (i.e. 5 predictor variables) black-box function that would have to be optimised is given the functional form described in Eq. 31.

$$h_{It} = \frac{d_1}{(d_1 + d_2 + d_3)} \quad \text{Eq. 29}$$

$$N_{It} = (N_{It}^l + (N_{It}^h - N_{It}^l) * s_1) * h_{It} \quad \text{Eq. 30}$$

$$\Delta m\% = f(\mathbf{x}) = f([s_1^i, s_2^i, s_3^i, b_1^i, b_2^i]) \quad \text{Eq. 31}$$

When generating the representative set of combinations to be evaluated for the 5D problem, direct Sobol sampling across all five predictor variables was unfair, since  $b_2$  spreads over a larger range as  $b_1$  increases, which biases sampling towards one corner of the triangular subspace (Figure 9A). Given the altitude method detailed above (Figure 8LR), a bias towards the bottom left as seen in Figure 9A would skew samples towards the citric acid system. To bias-correct the Sobol method, a custom sampler was programmed to use a rejection-sampling technique to distribute points quasi-randomly across the 2D parameter sub-space (Figure 9B).

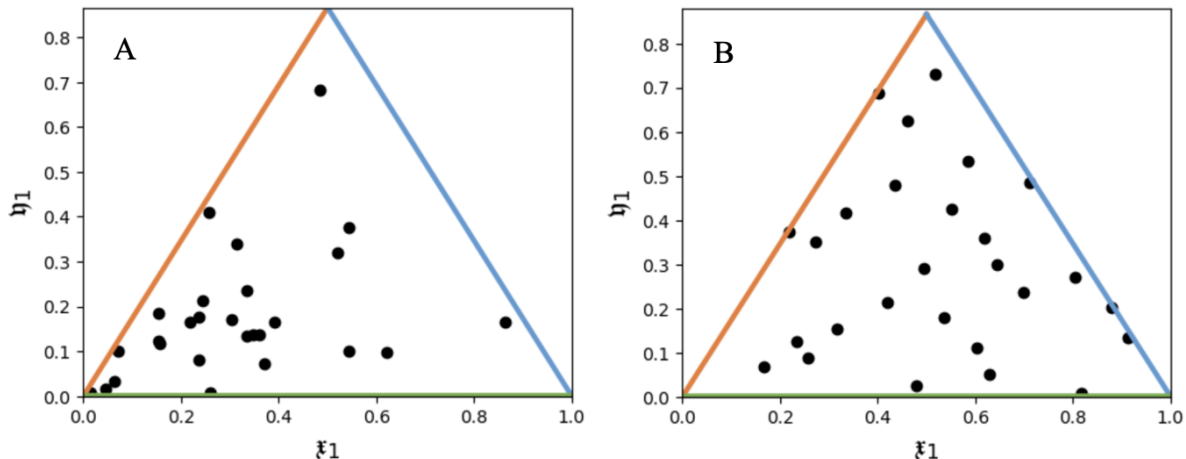


Figure 9 – Comparison of biased Sobol sampling (A) across the 2D parameter sub-space and bias-corrected Sobol sampling technique (B).

In a second stage, the custom sampler translates the points from the Sobol/rejection sampled Cartesian coordinates ( $\mathfrak{x}_1, \mathfrak{y}_1$ ) to the predictor variable values ( $b_1, b_2$ ) in the 2D parameter sub-space using the inverse function of that in Eq. 27. The distributions of the final predictor variables are quasirandom in 1D, apart from the perturbed variable  $b_1$  which likely exhibits a form of triangular distribution, and  $b_2$  which seems to exhibit a form of pseudorandom continuous distribution (Figure 10L).

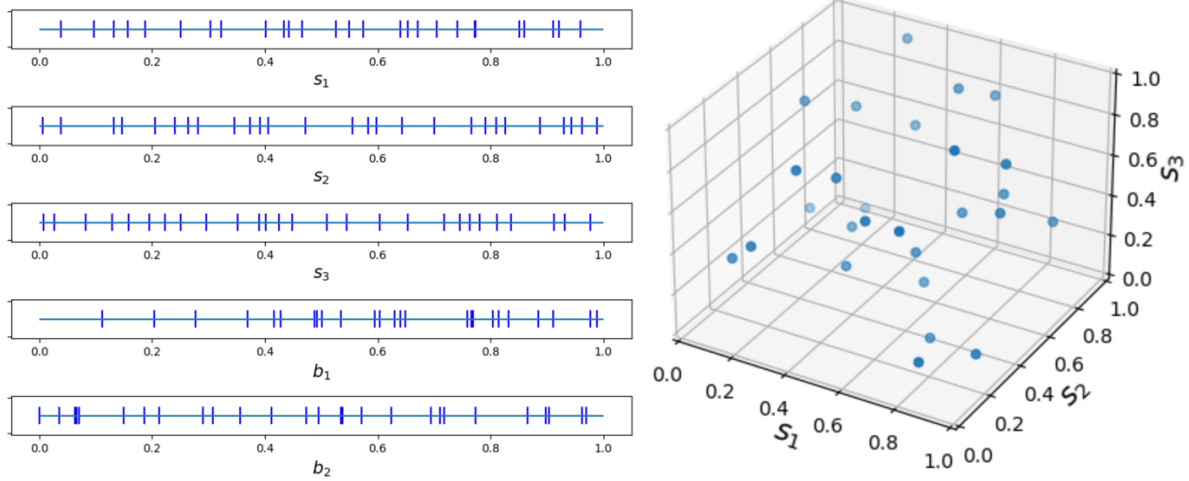


Figure 10 – Overview of samples generated by custom Sobol/Rejection sampler: Left, L: Distribution of samples across each of the predictor variables ranges in 1D. Right, R: Distribution of samples across the strength predictor variables 3D subspace.

Since quasirandom behaviour is retained between the strength predictor variables (Figure 10R), a pseudorandom connection between strength and balancing variables retained, and a representative balance between the three acid systems in  $b_1, b_2$  achieved through a custom Sobol/Rejection sampler this initial space-filling sampling technique was expected to be deployable for the 5D problem framed in Eq. 31. This was further supported by a comparison with an entirely pseudorandom sampling method for the 5D problem, where it was found that the custom Sobol/rejection sampling technique did provide a more robust coverage of the parameter space (See A8, A9, A10).

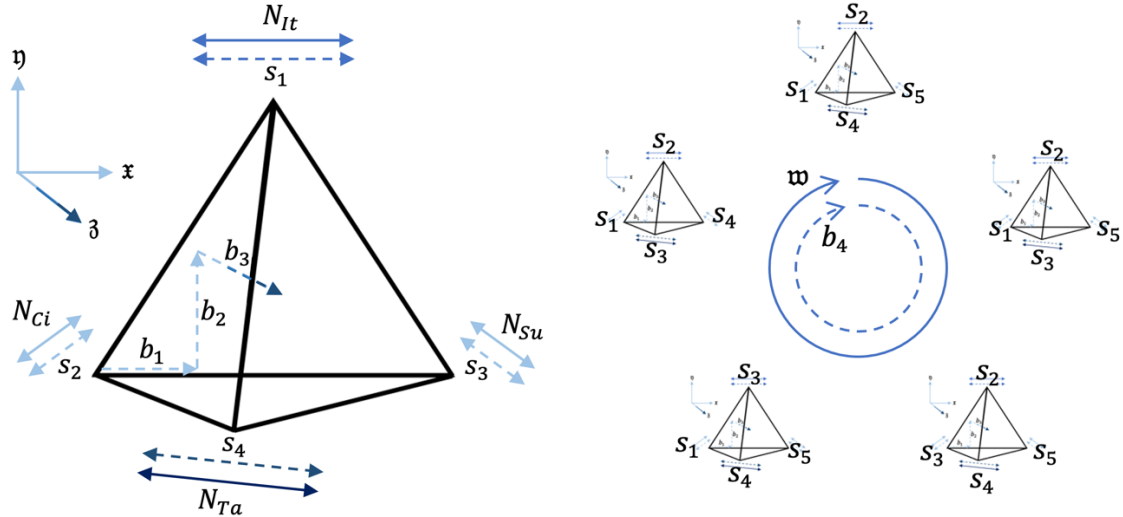


Figure 11 – Overview of 7D and 9D problems. Left, L: 7D tetrahedral 3D parameter sub-space for bounding of balancing parameters  $b_1, b_2, b_3$ . Right, R: 9D Naive 5-cell visualised in 3D for bounding of balancing parameters  $b_1, b_2, b_3, b_4$ .

With respect to dimensions higher than 5D, only 7D retained a naturally intuitive design for the balancing variables parameter sub-space: a tetrahedron (Figure 11L). A custom bias-corrected Sobol sampler could be built upon the same principles as for the 5D problem, with the altitude technique now applicable for distance from faces instead of lines. For 9D however, the next order of simplex, the 5-cell, provides few intuitive methods by which the now 4D parameter sub-space and the balancing predictor variables could be interlinked. A hypothesised technique by which this might be achieved was a circularisation of the 4<sup>th</sup> dimension  $w$  (Figure 11R) to be used as a balancing tool between multiple permutations of 3D sub-spaces, although naive early attempts to computationally prove retention of representative sampling have proven

fruitless. It is more likely that the 9D problem would be solved by carefully considering higher dimensional simplex coordinate systems (e.g. barycentric coordinates) and adapting the altitude method from 3D to 4D by finding distances from points to cells rather than faces.

### 2.3 – Black-Box Function Evaluation Method

To evaluate the black-box function during an optimisation a set of predictor variables' values  $\mathbf{x}$  must be passed to the function  $f$  and a target variable value  $\Delta m\%$  returned (e.g. Eq. 31); which is to say that a sample with a specific combination of stoichiometric variables' values for acid reactants (derived from  $\mathbf{x}$ ) must be reacted to find the percentage mass loss  $\Delta m\%$ . This section provides the manufacture/characterisation method by which this was achieved.

Initially, the optimisation program considers a combination of predictor variable values  $\mathbf{x}^i$  for a given sample  $i$  taken from the matrix  $\mathbf{X}$ , these individual values  $s_1^i, s_2^i, b_1^i$  are used to calculate the stoichiometric variables for citric acid  $N_{Ci}^i$ , and itaconic acid  $N_{It}^i$  (Glycerol's stoichiometric parameter is a constant and set to 1). At this point the user is prompted to weigh  $\sim 3$  ml of glycerol ( $\sim 3.78$  g) into a 25 ml beaker and return a mass of glycerol to the program; given this information and the stoichiometric ratios within the overall stoichiometric equation (Eq. 23), the program calculates citric and itaconic acid masses required for the test. The user can then manually weigh out these components, before adding them to the beaker of glycerol, this beaker and its contents are heated to 140 °C. During this heating process, the program prompts the user for the mass of a  $2 \times 2 \times 2$  cm silicone mould ( $m_m^i$ ). Once heated and complete dissolution is observed within the beaker, a  $\sim 3$  ml aliquot of prepolymer is retrieved by the user and pipetted into the silicone mould, the combined mass of which ( $m_{mp}^i$ ) would be inputted to the program before the mould is placed in the drying oven at 90 °C. Logging of mould mass and combined mould prepolymer masses allows the program to deduce prepolymer mass at the beginning of the polyesterification process  $m_p^i$  (Eq. 32).

$$m_p^i = m_{mp}^i - m_m^i$$

Eq. 32

If the case of the eight-sample Sobol-sampled predictor variable value matrix were to be considered, the lower bound of the index would be set to  $i = 1$  and the upper set to  $i = 8$ , and the combinations iterated through, and samples prepared accordingly and placed within the drying oven. From this point, the user is only prompted by the program to check the masses of these moulds and their contents once a day, this generates a dataset describing mass loss through time within the individual samples. During preliminary testing it was found that mass loss decayed in an exponential fashion, this allowed the program to fit an exponential curve as each daily data point was added. Simultaneously, the program would take linear tangents of the exponential from  $t = 0$  through till the current time in a search for an arbitrarily set goal gradient (-0.028 % hr<sup>-1</sup>), if discovered, the mass at that point would be considered the final mass of the thermoset ( $m_t^i$ ) and the test ended for that sample.

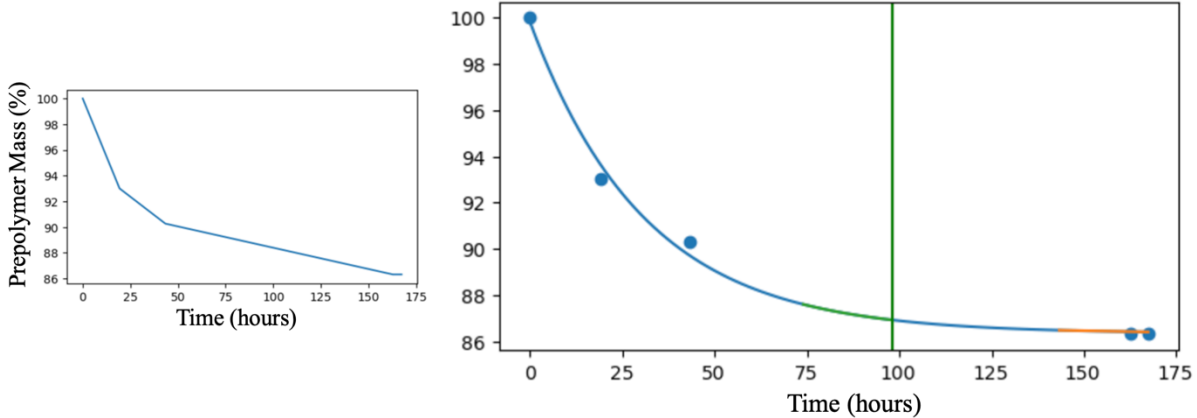


Figure 12 – Left: Prepolymer mass loss over time, data points connected by straight lines. Right: Prepolymer mass loss over time, data points scattered, and blue exponential curve fitted. Green vertical line shows time at which target gradient reached, and straight green tangent line exponential shows linear fit for last 24 hours of data. Orange line gives the latest 24hr tangent available at the time of graph drawing.

Using the final thermoset mass  $m_t^i$  and the original prepolymer mass  $m_p^i$  the program could then deduce the mass loss of a sample  $\Delta m^i$  (Eq. 33), and subsequently the absolute percentage mass loss  $\Delta m\%^i$  (Eq. 34); all percentage mass loss targets calculated were then finally placed in the main dataset  $\mathbb{D}$  governing the optimisation (Eq. 35).

$$\Delta m^i = m_p^i - m_t^i \quad \text{Eq. 33}$$

$$\Delta m\%^i = \frac{\Delta m^i \times 100}{m_p^i} = \frac{(m_p^i - m_t^i) \times 100}{m_p^i} \quad \text{Eq. 34}$$

$$\mathbb{D} = [\mathbf{X}, f(\mathbf{X})] = [\mathbf{X}, \Delta \mathbf{m}\%^i] = [[\mathbf{x}^{i=1}, \mathbf{x}^{i=2}, \dots], [\Delta m\%^{i=1}, \Delta m\%^{i=2}, \dots]] \quad \text{Eq. 35}$$

## 2.4 – Sequential Sampling Method

After the initial representative prior-initialising dataset  $\mathbb{D}^p$  generated from the space-filling sampling technique has been generated, the sequential sampling process is initiated. The sequential sampling method used is called Bayesian optimisation (BO)- this consists of a Bayesian statistical model for modelling the objective function, and an acquisition function for deciding where to sample next (69). Having utilised common python libraries to program the custom samplers required to representatively sample the parameter space, sequential sampling was implemented using the in-development Ax library (70) which effectively augments the BoTorch library (71) with higher-level functionality. This section gives an overview of how Bayesian optimisation operates, and details on what specific assumptions/methods were adopted.

### 2.4.1 – Bayesian Statistical Modelling Method

Since the sequential mechanism is Bayesian in nature, it abides by Bayes theorem (Eq. 36 & Eq. 37), where a posterior probability  $P(H|E)$  (updated probability of hypothesis  $H$  given new evidence  $E$ ) is equal to the prior probability (original probability of hypothesis) multiplied by the likelihood  $P(E|H)$  (probability of evidence given hypothesis) divided by the marginal probability  $P(E)$  (probability of evidence). As new evidence becomes available, the posterior probability is recycled into the equation as a prior alongside the new evidence and updated to a new posterior (72).

$$\text{posterior} = \frac{\text{prior} \times \text{likelihood}}{\text{marginal}} \quad \text{Eq. 36}$$

$$P(H|E) = \frac{P(H)P(E|H)}{P(E)} \quad \text{Eq. 37}$$

In BO the Bayesian statistical model used is called a Gaussian process (GP) regression model (73) (a form of Bayesian posterior probability distribution) and is derived via GP regression using the dataset  $\mathbb{D}$ , it is in effect a surrogate model which describes the link between a candidate array of predictor variables  $\mathbf{x}$  (e.g.  $\mathbf{x}^{i=8}$  from  $\mathbf{X}$ ) and the function evaluation  $f(\mathbf{x})$  (e.g.  $\Delta m_{\%}^{i=8}$  from  $\Delta \mathbf{m}_{\%}$ ) (Eq. 38) (57).

$$\hat{f}(\cdot): \mathbf{x} \mapsto f(\mathbf{x}) \quad \text{Eq. 38}$$

Importantly, because a GP is effectively an infinite-dimensional generalisation of multivariate normal distributions it inherits the properties of a conjugate prior (74), allowing the initial posterior GP (e.g.  $\mathcal{GP}^{i=8}$ ) to be recycled as a prior alongside new data (e.g.  $\mathbb{D} + [\mathbf{x}^{i=9}, \Delta m_{\%}^{i=9}]$ ) to generate an updated posterior GP (e.g.  $\mathcal{GP}^{i=9}$ ) in accordance with Bayes theorem (Eq. 36). This allows the surrogate model of the system to evolve as the number of iterations  $i$  increases, corresponding to the updating of beliefs considering new evidence which hallmarks all Bayesian methods.

Since a GP produces a posterior probability distribution on each  $f(\mathbf{x})$  which is normally distributed with mean  $\mu_i(\mathbf{x})$  and variance  $\sigma_i^2(\mathbf{x})$  (69), a GP could be sampled from to visualise the 95% Bayesian credible interval  $\mu_i(\mathbf{x}) \pm 1.96\sigma_i$  for  $f(\mathbf{x})$ - this interval contains  $f(\mathbf{x})$  with a 95% probability given the posterior distribution. In Figure 13A, a GP ( $\mathcal{GP}^{i=8}$ ) is fitted to the eight initial space-filling observations Sobol-sampled from across the range ([0,1]) of the single strength predictor variable  $s_1$  of the P(GIt) system. Figure 13A shows how the credible interval grows with distance from observations, quantifying uncertainty of the surrogate model's fit to the latent objective function. As an aside, GP's fit with wider credible intervals (Figure 13B) when measurement accuracies are specified (introducing noise within observations)- during the P(GCiIt) system optimisation no measurement noise was specified, it was therefore inferred by Ax during the sequential optimisation.

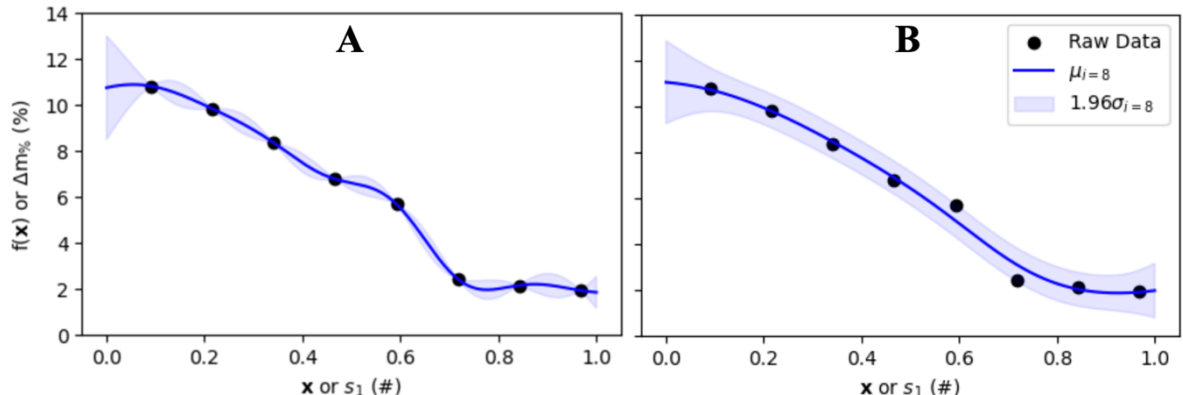


Figure 13 – Overview of Gaussian processes fitted to P(GIt) systems after 8 initial space-filling samples. A: noiseless observations assumed. B: average noise inferred and applied to each observation.  $\mu_i$  and  $\sigma_i$  are the mean and standard deviation predicted at  $x$  given the posterior distribution.

It is notable (although potentially beyond the scope of practical application desired in the 1<sup>st</sup> year) that covariance functions are a necessary component in the fitting of Gaussian processes as they encode our beliefs regarding the families of functions that are likely to fit the data being observed (73). In the P(GCiIt) system optimisation, the default BoTorch covariance function called the Matérn class of functions was used. Furthermore, covariance functions utilise hyperparameters  $\theta$  which must be tuned, the process of tuning being termed Gaussian process training- this tends to be achieved through Bayesian model selection or cross-validation techniques (73). A Bayesian model selection technique called log marginal likelihood was used during the P(GCiIt) chemical system optimisation (BoTorch default). Use of the default BoTorch settings in the P(GCiIt) chemical system optimisation were justified by the

smoothness of fit observed in lower dimensions with similar polyester systems, as seen for the P(GIt) chemical system in Figure 13.

#### 2.4.2 – Acquisition Function Method

Once a GP has been fit, an acquisition function is employed to direct the optimisation by suggesting where next to sample  $\mathbf{x}^+$  within the parameter space. This acquisition function  $\alpha$  maps any array of predictor variables  $\mathbf{x}$  to a scalar metric which we will call ‘value of potential sample’  $\gamma$  (Eq. 39), this function can then be directly optimised to find the highest value sample position  $\mathbf{x}^+$  in the parameter space at the current iteration (Eq. 40). When an acquisition function is fitted (for any sample iteration  $i$ ), it is dependent upon both the data observed so far  $\mathbb{D}$ , and the current GP’s hyperparameters  $\boldsymbol{\theta}$  (Eq. 39) (75).

$$\gamma = \alpha(\mathbf{x}) = (\mathbf{x}; \mathbb{D}, \boldsymbol{\theta}) \quad \text{Eq. 39}$$

$$\mathbf{x}^+ = \arg \max_{\mathbf{x} \in A} \alpha(\mathbf{x}) \text{ where } f: A \rightarrow \mathbb{R} \text{ and } A \subseteq \mathbb{R}^d \quad \text{Eq. 40}$$

An acquisition function is used as a tool for tackling a challenge termed the exploration-exploitation trade-off, where a sequential optimisation must balance between exploring undersampled regions of the parameter space using space-filling techniques and exploiting complex regions by placing samples in nonlinear subspaces (45). Quantification of uncertainty by the Gaussian process (visualised by  $1.96\sigma_{i=8}$  in Figure 13) provides information about regions that are ill-explored, whilst the mean ( $\mu_{i=8}$  in Figure 13) can indicate exploitable regions to the acquisition function.

In Figure 14A, points have been removed from an initial space-filling sampling exercise on the P(GIt) system to demonstrate how a GP quantifies uncertainty and influences the subsequently generated acquisition function. As the optimisation proceeds (Figure 14A→C) the acquisition function successfully balances exploration and exploitation during an attempted maximisation of the black-box function being investigated. In Figure 14B the acquisition function is encouraging sampling biased to within the parameter sub-space [0.0, 0.3], as the region is both underexplored (relatively large probability intervals) and exploitatively tempting (relatively high mean values). In Figure 14C, the acquisition function is still encouraging sampling within the [0.0, 0.3] sub-space, although the  $\gamma$  peak has reduced substantially indicating the region becoming progressively better sampled, this will steadily bias the acquisition function away from the region in following iterations.

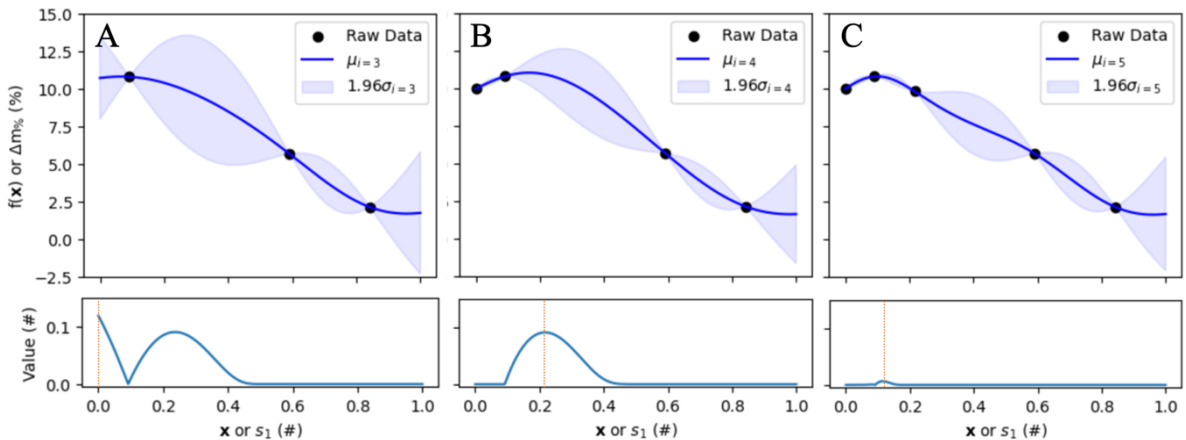


Figure 14 – Visualisation of a sequential optimisation’s progression, with the growing dataset and associated GPs plotted in the upper three graphs, whilst the linked acquisition functions evaluated from these posterior distributions are plotted separately below. Orange vertical lines indicate the suggested next point to sample  $\mathbf{x}^+$ .

There exist three common acquisition functions in literature; firstly, ‘probability of improvement’ (PI), which maximises the probability of improving over the current best value

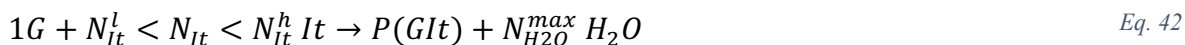
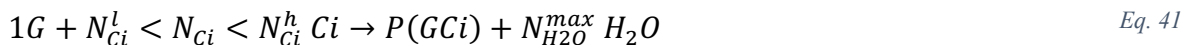
(76). Secondly, ‘expected improvement’ (EI), which seeks to maximise the expected improvement over the current best (75). Thirdly, ‘GP upper confidence bounds’, which exploit upper confidence bounds so that acquisition functions minimise regret during iterative optimisation (77). In the final P(GCiIt) optimisation, both the PI and EI methods were trialled and compared; the particular form of EI adopted was termed batch noisy expected improvement (78).

## 2.5 – P(GCiIt) System Optimisation

To address the hypothesis posited at the start (“Bayesian optimisation can be used to increase the sample efficiency when optimising the properties of BBAPTs”) common deterministic space-filling techniques (non-sequential optimisation) were trialled on a limited number of samples. Best tuples of target variable  $f(\mathbf{x}^*)$  and predictor variables  $\mathbf{x}^*$  yielded by these techniques were considered benchmarks above which the Bayesian sequential optimisation technique would seek to improve given the same number of samples. The P(GCiIt) chemical system was selected to be optimised given its relatively complicated parameter-space (yielding a non-trivial optimisation problem), which consisted of the normalised predictor variables:  $s_1$  controlling strength of itaconic acid stoichiometry ([0,1]- low to high strength),  $s_2$  controlling strength of citric acid stoichiometry ([0,1]- low to high strength), and  $b_1$  balancing dominance of citric acid over itaconic acid systems ([0,1]- low to high citric acid dominance). All optimisations were carried out using the BO4BT python package (79), which automates many of the aspects of BBAPT sequential optimisation, this was programmed using all the method described in Chapter’s 2.1 through 2.4.

### 2.5.1 – Theoretical Maximum Mass Loss

To contextualise the optimisations carried out, theoretical maximum mass losses were calculated for the P(GCiIt) system. Given the constraints on stoichiometry assumed earlier ( $N_{Ci}^l = 0.5, N_{It}^l = 1, N_{Ci}^h = N_{It}^h = 2$ ), the overall stoichiometric equation (Eq. 23), and the assumption that all three alcohol groups on every glycerol molecule bond and form 3 molecules of water ( $N_{H2O}^{max} = 3$ ), two edge-case stoichiometric equations are possible (Eq. 41, Eq. 42).



If a constant of 1 g ( $m_k$ ) is assumed for glycerol mass and molar mass of glycerol ( $M_{Gl}$ , 92.05 g/mol), citric acid ( $M_{Ci}$ , 192.03 g/mol), and itaconic acid ( $M_{It}$ , 130.03 g/mol) taken into consideration, then upper and lower bounds of acid mass ( $m_{Ci}^l, m_{Ci}^h, m_{It}^l, m_{It}^h$ ) can be calculated for each edge-case. Furthermore, if it is taken that all glycerol and itaconic acid were to be bound within a BBAPT thermoset by the end of the polycondensation, then theoretical upper and lower ultimate masses of thermoset ( $m_{P(GCi)}^{Min}, m_{P(GCi)}^{Max}, m_{P(GIt)}^{Min}, m_{P(GIt)}^{Max}$ ) can be calculated (Eq. 43, Eq. 44).

$$\frac{m_k \times N_{Ci}^l \times M_{Ci}}{M_{Gl}}, \frac{m_k \times N_{Ci}^h \times M_{Ci}}{M_{Gl}} = m_{Ci}^l, m_{Ci}^h \rightarrow m_{Ci}^l + m_k, m_{Ci}^h + m_k = m_{P(GCi)}^{Min}, m_{P(GCi)}^{Max} \quad Eq. 43$$

$$\frac{m_k \times N_{It}^l \times M_{It}}{M_{Gl}}, \frac{m_k \times N_{It}^h \times M_{It}}{M_{Gl}} = m_{It}^l, m_{It}^h \rightarrow m_{It}^l + m_k, m_{It}^h + m_k = m_{P(GIt)}^{Min}, m_{P(GIt)}^{Max} \quad Eq. 44$$

When molecular mass of water is considered ( $M_{H2O}$ , 18.02 g/mol) then the maximum mass of water that can be generated  $m_{H2O}^{Max}$  in any of the end cases can be calculated (Eq. 45).

$$\frac{m_k \times N_{H2O}^{max} \times M_{H2O}}{M_{Gl}} = \frac{1 \times 3 \times 18.02}{92.05} = m_{H2O}^{Max} \quad Eq. 45$$

Maximum expected water loss (mass loss,  $\Delta m\%$ ) as a percentage of the maximum theoretical thermoset masses can be calculated for each of the edge-cases yielding the theoretical

maximum loss  $\Delta m_{\%}^{\dagger} = 28.92\%$  (Eq. 46, Eq. 47). Note, that  $\Delta m_{\%}^{\dagger}$  is likely to be unachievable and that a lower unknown global optimum given the constraints  $\Delta m_{\%}^*$  is still the true goal of these optimisation routines.

$$\frac{m_{H_2O}^{Max} \times 100}{m_{P(GCi)}^{Max}} < \Delta m_{\%} < \frac{m_{H_2O}^{Max} \times 100}{m_{P(GCi)}^{Min}} = 11.41 < \Delta m_{\%} < 28.92 = \Delta m_{\%} < \Delta m_{\%}^{\dagger} \quad Eq. 46$$

$$\frac{m_{H_2O}^{Max} \times 100}{m_{P(GIt)}^{Max}} < \Delta m_{\%} < \frac{m_{H_2O}^{Max} \times 100}{m_{P(GIt)}^{Min}} = 15.40 < \Delta m_{\%} < 24.48 \quad Eq. 47$$

### 2.5.2 – Benchmarking Optimisations

Three space-filling techniques were used as benchmark optimisations, these were grid-sampling (SF-Gr), quasirandom sampling (SF-QR) using the Sobol method, and pseudorandom sampling (SF-PR). As the number of samples  $N_{Gs}$  required for a grid sampling exercise scales exponentially (Eq. 48) with the number of dimensions  $d$  considered (when ticks  $t$  along an axis is held constant), a compromise between size of experiment and coverage of parameter space was arbitrarily set at 27 samples. This value was adopted as the maximum allowable number of samples within any optimisation technique tested,  $N_s = 27$ .

$$N_{Gs} = t^d \quad Eq. 48$$

In Figure 15 the relative performance of the three techniques becomes apparent when 27 samples are requested from across the 3D parameter space, with representativity hierachised in the following order: SF-PR < SF-QR < SF-Gr (where “less < more” representative).

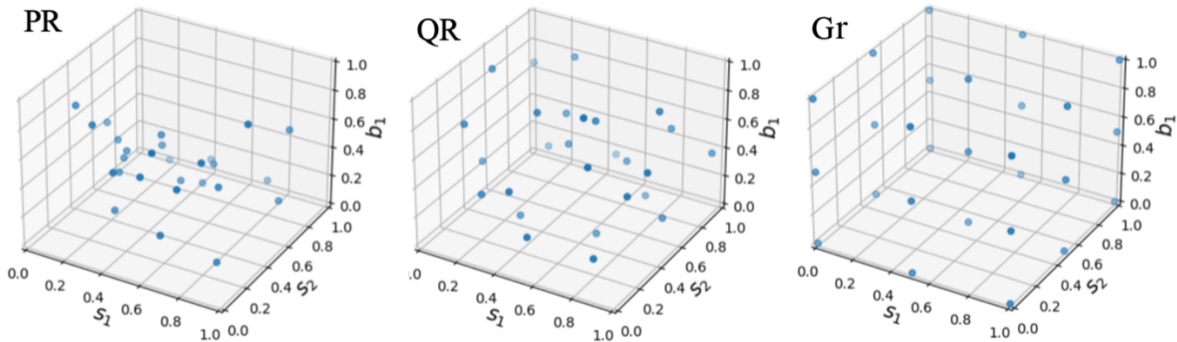


Figure 15 – Comparison of space-filling sampling techniques and distribution of 27 samples across the entire 3D parameter space of the P(GCiIt) problem. G: Grid sampling technique, QR: Quasirandom sampling technique, PR: Pseudorandom sampling technique.

Having used the three space-filling techniques to produce three sets of 27 combinations of predictor variables  $\mathbf{X}_{PR}, \mathbf{X}_{QR}, \mathbf{X}_{Gr}$ , the black-box function describing the P(GCiIt) system (Eq. 24) was evaluated for each of these sets to generate three separate arrays of target values  $f(\mathbf{X}_{PR}), f(\mathbf{X}_{QR}), f(\mathbf{X}_{Gr})$ . Table 1 supports the previously suggested hierarchy since SF-PR < SF-QR < SF-Gr in terms of standard deviation- the larger the standard deviation in targets the more representative/diverse the set of combinations evaluated. The same hierarchy exists with respect to the maximum values obtained; this is explained by the fact that greater variance within targets would be directly correlated with higher numbers of extremely low and high target values having been discovered.

Table 1 – Overview of space-filling benchmarking optimisation results with respect to the targets obtained after 27 samples. SF-Gr: Space-filling grid sampler. SF-QR: Space-filling quasirandom sampler. SF-PR: Space-filling pseudorandom sampler.

Trial	Samples (#)	Max, $\Delta m^\circ$ or $f(\mathbf{X})^\circ$ (%)	Mean, $\mu_{f(\mathbf{X})}$ (%)	Standard Deviation, $\sigma_{f(\mathbf{X})}$ (%)
SF-Gr	27	16.24	11.93	1.66
SF-QR	27	14.55	12.34	1.43
SF-PR	27	14.01	12.54	0.88

### 2.5.3 – Bayesian Optimisations

Of the many variables likely to affect the efficacy of a sequential optimisation with a sample limit ( $N_s = 27$ ), three variables were focussed upon. Firstly, space-filling to sequential sample ratio, which was ratio of samples obtained from space-filling sampling (used in the prior-forming dataset) to samples being sequentially sampled (taken during sequential optimisation). Secondly, acquisition function deployed, which was the type of acquisition function used to evaluate the fitted gaussian process at each iteration. Thirdly, samples per iteration  $N_s^i$ , which was the maximum number of function evaluations (samples) that could take place at any given iteration.

When considering the space-filling to sequential sample ratio two ratios were settled upon for trials, one set at 3:7 (30% space-filling) and the other at 3:2 (60% space-filling). Given this and the sample limit  $N_s$  two representative datasets were generated to be used for prior-initialisation based on 8 ( $\mathbb{D}_{i=8}^p$ ) and 16 ( $\mathbb{D}_{i=16}^p$ ) quasirandom Sobol samples respectively (Figure 16).

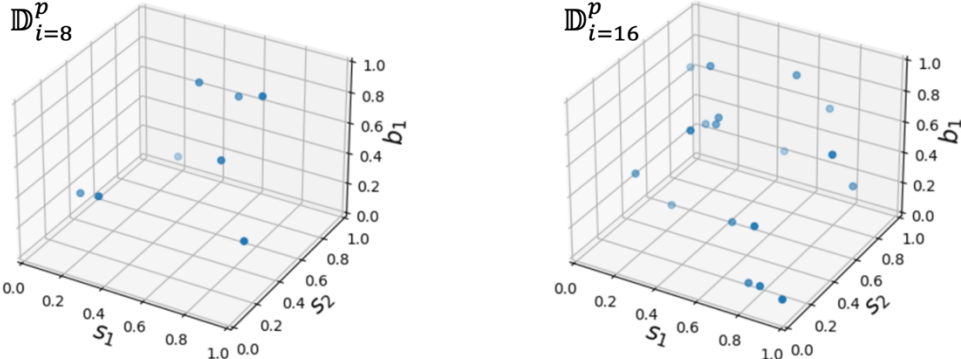


Figure 16 – Visualisation of the two representative prior datasets quasirandomly across the 3D parameter space of the  $P(GCIt)$  system.  $\mathbb{D}_{i=8}^p$ : Eight sample prior dataset.  $\mathbb{D}_{i=16}^p$ : Sixteen sample prior dataset.

Two acquisition functions were considered, one being the probability of improvement method (PI) and the other being the expected improvement method (EI). Three optimisations with different samples per iteration were begun ( $N_s^i = 1$ ,  $N_s^i = 2$ , and  $N_s^i = 3$ ) although due to the temporal expense of black-box function evaluations only the  $N_s^i = 3$  optimisations reached the sample limit  $N_s$  by the end of the year. The slow-stepping trials ( $N_s^i = 1$ ,  $N_s^i = 2$ ) which are still incomplete are therefore not discussed within this section of the report although their current progress can be found within the appendix. Since only the  $N_s^i = 3$  permutation is considered, only four Bayesian optimisations were completed: Trials “BO-PI-D8” and “BO-PI-D16” both using the PI acquisition function and  $\mathbb{D}_{i=8}^p$  and  $\mathbb{D}_{i=16}^p$  as prior-initialisation datasets respectively. Trials “BO-EI-D8” and “BO-EI-D16” both used the EI acquisition function and  $\mathbb{D}_{i=8}^p$  and  $\mathbb{D}_{i=16}^p$  as prior-initialisation datasets respectively. These tests and their findings are summarised in Table 2. Note that given there are  $N_s^i = 3$  samples per trial for these optimisations, the  $\mathbb{D}_{i=8}^p$  and  $\mathbb{D}_{i=16}^p$  optimisations go through 19 and 11 sequential samples respectively. Furthermore, these optimisations would go through 6 and 3 full iterations (i.e.

each consisting of 3 samples) respectively, and 1 final partial iteration (consisting of 1 and 2 samples respectively).

Table 2 – Overview of Bayesian optimisation results with respect to the targets obtained after 27 samples (excl. SF-D8 and SF-D16 with 8 and 16 samples respectively). SF: Space-filling method. BO: Bayesian optimisation method. D8/16: 8/16-sample representative dataset. PI: Probability of improvement acquisition function. EI: Expected improvement acquisition function. SF-D8/16: Prior-initialising space-filling datasets are also included here.

Trial	Sequential Samples (#)	Max, $\Delta m^\circ$ (%)	Mean, $\mu_{f(x)}$ (%)	Standard Deviation, $\sigma_{f(x)}$ (%)
SF-D8	n/a	14.01	12.82	1.04
SF-D16	n/a	15.38	13.15	1.26
BO-PI-D8	19	16.67	12.50	1.63
BO-EI-D8	19	17.99	13.67	1.91
BO-PI-D16	11	15.38	12.73	1.29
BO-EI-D16	11	15.74	13.16	1.57

#### 2.5.4 – Cross-Comparison of Optimisations

Capability of different Bayesian optimisations to discover values approaching the theoretical maximum  $\Delta m^\dagger = 28.92\%$  was cross-compared using graphs describing the progression of best global maximum values  $\Delta m^\circ$  discovered. In Figure 17 the two Bayesian optimisations using the  $\mathbb{D}_{i=16}^p$  prior-initialising dataset are compared in terms of their  $\Delta m^\circ$  progression, one employs the PI acquisition function (BO-PI-D16, green line) whilst the other uses EI (BO-EI-D16, blue line). Benchmark  $\Delta m^\circ$  values are also plotted (horizontal dashed lines) for the various space-filling techniques (Grid, Quasirandom, and Pseudorandom) which used the full number of samples ( $N_s = 27$ ) in a single iteration; the sample limit  $N_s$  is visualised as a dashed black vertical line.

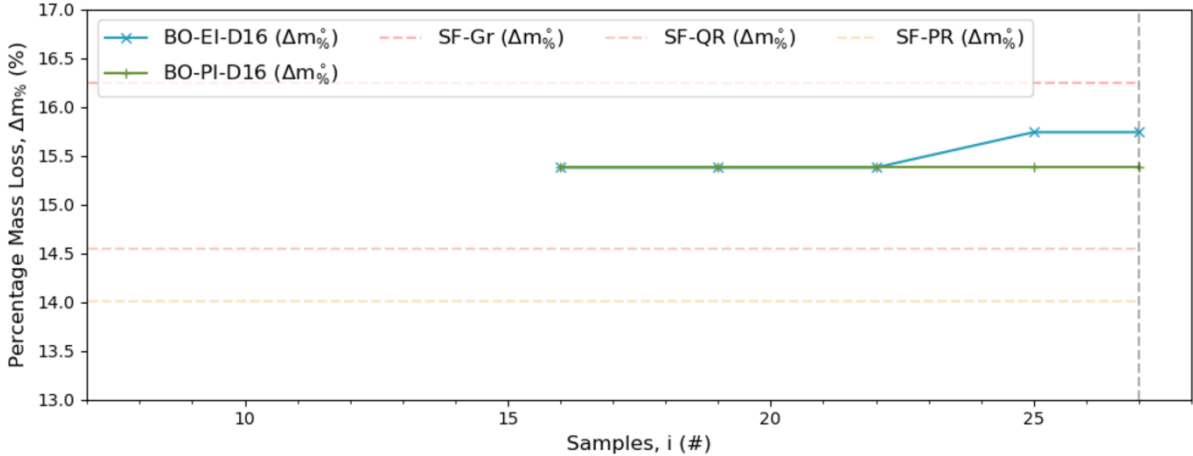


Figure 17 – Graph describing optimisation progression with respect to best global optimum  $\Delta m^\circ$  discovered at any given iteration for BO-EI-D16 and BO-PI-D16. Black dashed vertical line denotes  $N_s$ . Crosses or pluses distributed along solid lines denote the  $\Delta m^\circ$  at the end of an iteration. SF-Gr/QR/PR: Space-filling Grid/Quasirandom/Pseudorandom techniques. BO: Bayesian optimisation method. PI: Probability of improvement acquisition function. EI: Expected improvement acquisition function. D16: 16-sample prior-initialising dataset.

Both optimisations are initialised at  $i = 16$  when the first Gaussian process is fit to the prior-initialising dataset  $\mathbb{D}_{i=16}^p$  and the first three sets of predictors are suggested for evaluation. At this stage the highest current values of  $\Delta m\%$  ( $\Delta m^\circ$ ) for each optimisation will have come from their common initialisation dataset  $\mathbb{D}_{i=16}$ , hence their common start points in Figure 17. After a week baking in a drying oven at 90 °C, the mass loss is evaluated for each of these initial samples and placed in the optimisation’s dataset  $\mathbb{D}_{i=16}$  before the next iteration begins, if any improvements upon the current best are found then  $\Delta m\%$  is updated and this becomes apparent

in Figure 17 as an uptick. At  $i = 22$  the two progressions diverge, with BO-EI-D16 rising 0.36% higher than BO-PI-D16 with respect to  $\Delta m^\circ$  by  $i = 25$ ; this shows that one of the three sequential samples taken during the third Bayesian iteration of BO-EI-D16 made an improvement on the current best value. By the end of the two optimisations ( $i = 27$ ), BO-PI-D16 failed to improve its  $\Delta m^\circ$  whilst BO-EI-D16 improved its  $\Delta m^\circ$  from 15.38% to 15.74%. Neither of the two Bayesian optimisations improved beyond the strongest baseline set by the grid sampler ( $\Delta m^\circ = 16.24$ ).

In Figure 18,  $\Delta m^\circ$  progression for the two Bayesian optimisations leveraging the smaller  $\mathbb{D}_{i=8}^p$  prior-initialising dataset are graphed, one employs the PI acquisition function (BO-PI-D8, light green line) whilst the other uses EI (BO-EI-D8, light blue line). Since both use the same prior-initialising dataset they share a common initial  $\Delta m^\circ$  value (14.01%) at  $i = 8$ . In the first three Bayesian iterations BO-EI-D8 shows a monotonic rise in  $\Delta m^\circ$  values discovered; it marginally surpasses the quasirandom benchmark (SF-QR) after a single iteration and comfortably surpasses the grid benchmark (SF-Gr) after its third iteration. Values for  $\Delta m^\circ$  discovered by BO-PI-D8 marginally surpass the SF-QR benchmark after 5 iterations, and marginally surpasses SF-Gr benchmark in its final partial iteration.

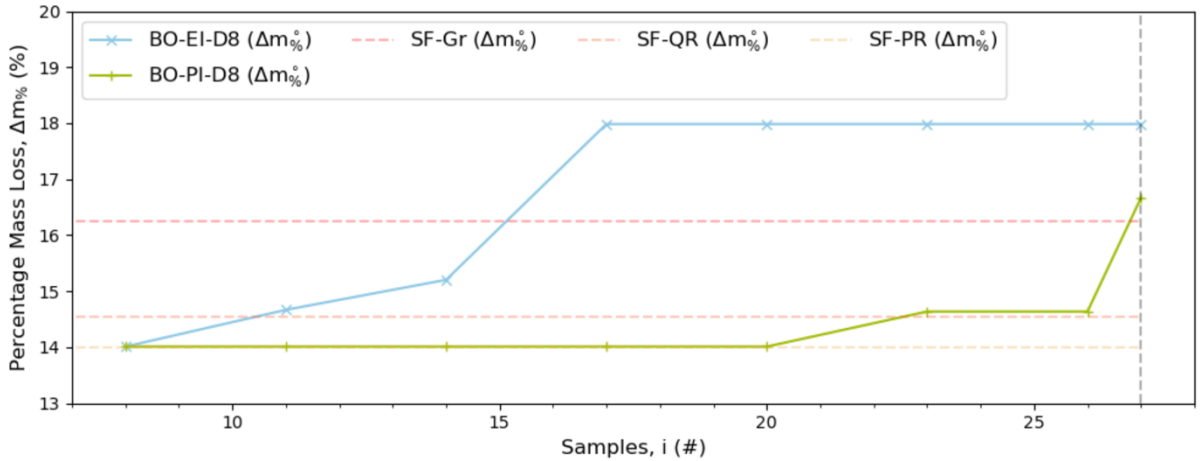


Figure 18 – Graph describing optimisation progression with respect to best global optimum  $\Delta m^\circ$  discovered at any given iteration for BO-EI-D8 and BO-PI-D8. Black dashed vertical line denotes  $N_s$ . Crosses or pluses distributed along solid lines denote the  $\Delta m^\circ$  at the end of an iteration. SF-Gr/QR/PR: Space-filling Grid/Quasirandom/Pseudorandom techniques. BO: Bayesian optimisation method. PI: Probability of improvement acquisition function. EI: Expected improvement acquisition function. D8: 8-sample prior-initialising dataset.

#### Observation 1 – Prior-Forming Dataset Size Effect

Bayesian optimisations leveraging the smaller prior-initialising dataset ( $\mathbb{D}_{i=8}^p$ ) discovered  $\Delta m^\circ$  values higher than the best benchmark (SF-Gr) before reaching the sample limit  $N_s$ . The  $\mathbb{D}_{i=8}^p$  optimisations used a sample ratio of 30%:70% between space-filling (samples in  $\mathbb{D}^p$ ) and sequential (samples  $N_s^i$ ) whilst  $\mathbb{D}_{i=16}^p$  used a 60%:40% ratio. Taken together, this shows that Bayesian optimisation procedures with more iterations (higher numbers of sequential samples) tend to discover better values for  $\Delta m^\circ$  before the arbitrary stopping point. This deduction will have limits since Bayesian optimisations provided an extremely small and unrepresentative prior-initialising dataset can be biased away from more productive global optimisation during the early stage of its sampling.

#### Observation 2 – Acquisition Function Effect

Optimisation BO-EI-D8 discovered improved  $\Delta m^\circ$  values more rapidly than the BO-PI-D8 optimisation, and therewith surpassed the best benchmark (SF-Gr) earlier in the sequential sampling process. It could therefore be posited that Bayesian optimisations using the expected improvement acquisition function are more sample efficient than those using probability of

improvement. This conclusion is supported by similar trends exhibited by BO-EI optimisations in the incomplete optimisation trials where  $N_s^i$  was set at 1 and 2 (A13, A14).

*Observation 3 – Bayesian Optimisation Sample Efficiency*

A Bayesian optimisation which stepped at a rate of  $N_s^i = 3$  per iteration, leveraged an EI acquisition function, and split its  $N_s$  30%:70% between a quasirandom prior dataset and sequential sampling (BO-EI-D8), could generate values for  $\Delta m^\circ\%$  higher than those obtained with a grid, quasirandom, or pseudorandom sampling space-filling techniques using the same ultimate number of samples  $N_s$ . This shows that Bayesian optimisation, when set up correctly, can optimise more sample-efficiently across a parameter space than space-filling techniques used in isolation- this supports the originally stated hypothesis to be investigated this year.

*Observation 4 – Stochastic Sampling Problem*

When the best  $\Delta m^\circ\%$  values are compared between the SF-D16 ( $\mathbb{D}_{i=16}^p$  prior-initialising dataset) and SF-QR (space-filling quasirandom benchmark) trials, both of which use a quasirandom Sobol space-filling sampling technique, SF-D16 obtains a better result despite using substantially less samples. This may simply be explained by the stochastic nature of drawing samples using a Sobol sampler; the two trials show similar spread when compared (A12) and the mean of SF-D16 happens to be greater than any of the space-filling trials carried out. Another possible explanation would be experimenter bias- a 3D plot of quasirandomly sampled points for SF-D16 was visualised before the optimisation commenced, the experimenter could have re-sampled the space if not satisfied with the representativity of the sampling, meanwhile none of the benchmark trials were visualised before the samples were evaluated. This hypothesis would be supported by the slightly more swarmed SF-QR data points when compared alongside the SF-D16 points (A12). Fortunately, even if such a bias was the case, the fact that  $\Delta m^\circ\%$  fell below that of the strongest benchmark (SF-Gr) allowed for the Bayesian optimisation techniques to prove their capability.

*Observation 5 – Global Optimum Estimation,  $\Delta m^\ast\%$*

The highest value for mass loss  $\Delta m^\circ\%$  discovered by any sequential Bayesian optimisation technique within the  $N_s = 27$  limit was the BO-EI-D8 optimisation which obtained a value of  $\Delta m^\circ\% = 17.99\%$ ; this can be alternatively written as  $0.62\Delta m^\dagger\%$  (as the theoretical limit is  $\Delta m^\dagger\% = 28.92\%$ ) whilst the grid sample benchmark obtained  $0.56\Delta m^\dagger\%$  (SF-Gr,  $\Delta m^\circ\% = 16.24\%$ ). Interestingly, BO-PI-D8 surpassed both these values with a value of  $0.72\Delta m^\dagger\%$  ( $\Delta m^\circ\% = 20.78\%$ ), although this was obtained in the final partial iteration after the sample cut-off  $N_s$  (A11, A15). It can therefore be stated that after 292 separate sample evaluations of the black-box function across all optimisations carried out (A16),  $\Delta m^\ast\% = 20.78\%$  obtained by the BO-EI-D8 optimisation is proffered as the best estimate of the global optimum for the P(GCiIt) system.

*Observation 6 – Optimum Stoichiometry Derivation*

By taking an optimisation's best set of predictors  $x^\circ$  and the associated best discovered value  $\Delta m^\circ\%$ , a stoichiometry of the best samples generated can be derived (Table 3). Furthermore, by multiplying up and rounding molar values sensibly, underlying structure of the polymers can be speculated.

Table 3 – Stoichiometries of the best performing samples associated with  $\Delta m_{\%}^{\dagger}$  and  $x^{\circ}$  of the benchmark optimisations and the Bayesian optimisations using the  $\mathbb{D}_{i=8}^p$  prior-initialising dataset.

Trial	$\Delta m_{\%}^{\dagger}$ Fraction	Derived Stoichiometry / Simplified Stoichiometry
SF-PR	$0.48\Delta m_{\%}^{\dagger}$	$1 G + 0.64 Ci + 0.40 It \rightarrow P(GCiIt) + 1.44 H_2O$ $\approx 3 G + 2 Ci + 1 It \rightarrow P(GCiIt) + 4 H_2O$
SF-QR	$0.50\Delta m_{\%}^{\dagger}$	$1 G + 0.18 Ci + 0.82 It \rightarrow P(GCiIt) + 1.5 H_2O$ $\approx 5 G + 1 Ci + 4 It \rightarrow P(GCiIt) + 8 H_2O$
SF-Gr	$0.56\Delta m_{\%}^{\dagger}$	$1 G + 0.50 Ci + 0.00 It \rightarrow P(GCiIt) + 1.68 H_2O$ $\approx 10 G + 5 Ci \rightarrow P(GCiIt) + 17 H_2O$
BO-EI-D8	$0.62\Delta m_{\%}^{\dagger}$	$1 G + 0.49 Ci + 0.03 It \rightarrow P(GCiIt) + 1.86 H_2O$ $\approx 10 G + 5 Ci \rightarrow P(GCiIt) + 19 H_2O$
BO-PI-D8	$0.72\Delta m_{\%}^{\dagger}$	$1 G + 0.78 Ci + 0.37 It \rightarrow P(GCiIt) + 2.16 H_2O$ $\approx 10 G + 8 Ci + 4 It \rightarrow P(GCiIt) + 22 H_2O$

In the case of SF-PR and SF-QR, it was found that the number of water molecules generated (i.e. number of ester bonds generated) did not account for the number of molecules and their associated functional groups; this indicated a form of partial or incomplete polymerisation within the bulk of the material. This incomplete polymerisation is visualised in Figure 19 by taking the simplified stoichiometric equations from Table 3 and combining the molecules in such a way as to satisfy the equation; note that for SF-PR/QR there are a range of different solutions, and so an arbitrary one is picked to be visualised.

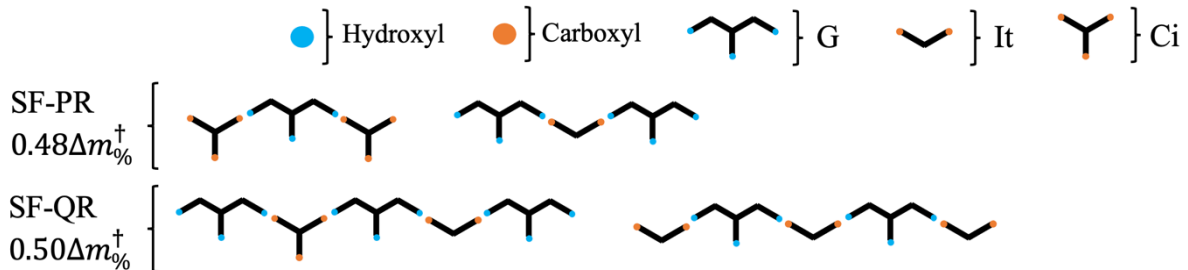


Figure 19 – Illustration of partial/incomplete polymerisations occurring within the best samples generated by the benchmark optimisations SF-PR and SF-QR. The key includes hydroxyl functional groups, carboxyl functional groups, G for glycerol molecules, It for itaconic acid molecules, and Ci for citric acid molecules

For SF-Gr, enough moles of water were generated to account for complete bonding of all molecules within a wider polymeric structure. Furthermore, when the stoichiometric equation for 10 moles of glycerol is visualised in Figure 20L, it becomes clear that there are more moles of water than bonds possible between the reactants, this suggests branching of the polymer as it grows. Subsequently, a repeat unit is ventured in Figure 20R- two moles of glycerol for every one mole of citric acid with one guaranteed bond to another repeat unit, whilst a second possible bond may exist. This second bond's existence can be described by a Bernoulli trial with sample space  $\Omega = \{NoBond, Bond\}$ , a binary random variable Q with states  $q \in \{0,1\}$ , a sample space mapping  $f_q: Q \rightarrow \Omega$ , and a random variable distributed in accordance with Bernoulli distribution  $Q \sim Ber(\mu)$  which takes the continuous parameter  $\mu \in [0,1]$  which in this case is  $\mu = 0.4$ .

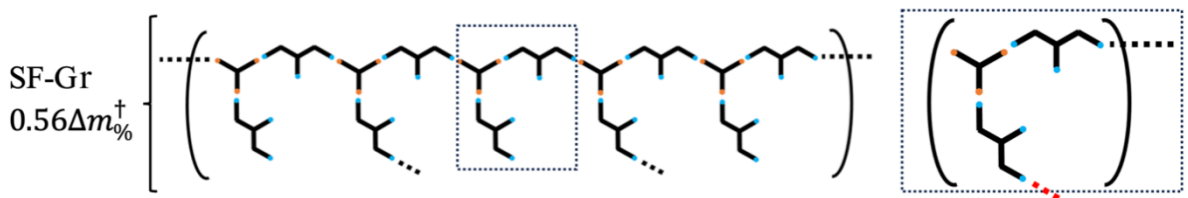


Figure 20 – Illustration of polymerisation occurring within the best sample generated by the SF-Gr benchmark optimisation. Left, L: Visualisation of stoichiometric equation with ten moles of glycerol, five repeat units within. Right, R: A single possible repeat unit for this branching polymer.

When BO-EI-D8's best sample's simplified stoichiometry is calculated for 10 moles of glycerol, and a visualisation like that of SF-Gr is produced (Figure 21L), it is found that the even more moles of water are unaccounted for making the chance of a branching at every given repeat unit more likely (i.e.  $\mu = 0.6$ ). Unlike SF-Gr's optimal result, BO-EI-D8's sample incorporates small ratios of itaconic acid, this may have impacted the polymer's conformation in such a way as to increase the likelihood of branching or successful crosslinking in the repeat units (Figure 21R).

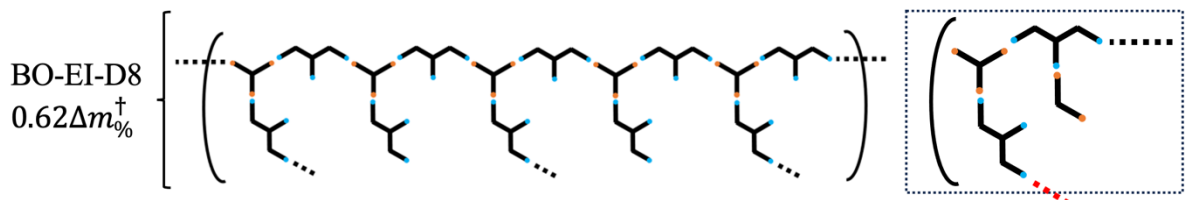


Figure 21 – Illustration of polymerisation occurring within the best sample generated by the BO-EI-D8 optimisation. Left, L: Visualisation of stoichiometric equation with ten moles of glycerol, five repeat units within. Right, R: A rare occurrence within the backbone of the polymer where an itaconic acid molecule is incorporated.

In BO-PI-D8's best sample's stoichiometry it is found that there exist enough water molecules to account for bonding between all the reactant molecules, but only one spare water molecule to have been derived from a polymerising esterification reaction. When this is visualised for 10 moles of glycerol, it becomes clear that the polymer being formed may be more linear in nature than branched. This breakthrough sample obtained just after the end of the  $N_s = 27$  sample cut off by the BO-PI-D8 could mark the discovery by the Bayesian optimisation of an alternate tactic for increased mass loss; one of linear polyester formation- which increases the share of glycerol hydroxyl sites esterified therewith increasing the mass loss through esterification-derived water genesis.

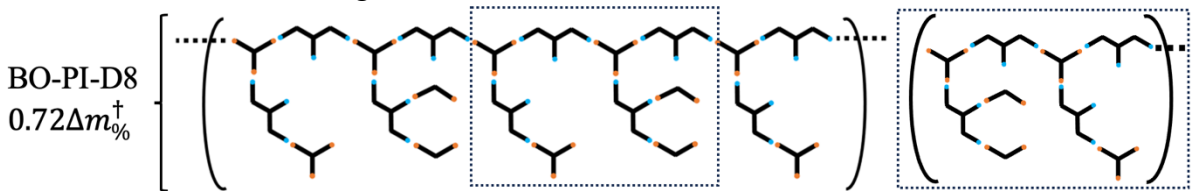


Figure 22 – Illustration of polymerisation occurring within the best sample generated by the BO-PI-D8 optimisation. Left, L: Visualisation of stoichiometric equation with ten moles of glycerol, two and a half repeat units within. Right, R: An image of what the repeat unit may look like.

Importantly, it must be caveated that all the above structures and associated conclusions are premised on the notion that the polymerisations are complete, with all reactants incorporated into the macromolecules described. If these reactions did not use up every molecule of triol, triacid and diacid during these reactions, then other structures may have emerged which were not predicted by looking at the general stoichiometries. Furthermore, each of the visualised structures are one of many that could satisfy the general equations.

#### Concluding Remarks

The 1<sup>st</sup> year's work culminated in generally supporting the originally posited working hypothesis- Bayesian optimisation was found to be capable of increasing sample efficiency

with respect to the optimisation of desirable properties in BBAPT materials, as both Bayesian optimisation routines based on the  $\mathbb{D}_{i=8}^p$  prior-initialising datasets outperformed the benchmark optimisations. Yet, while it is true that the desired metric of BBAPT mass loss was optimised efficiently and effectively by Bayesian optimisation within the sample limit  $N_s$ , the same cannot strictly be said for samples obtained without. The unexpected discovery made by the BO-PI-D8 optimisation was the formation of a linear polyester (rather than thermosetting), which throws doubt on whether these optimisations would have continued optimising the desired property in biodegradable bio-based aliphatic thermosets or whether they would rather have converged upon an alternate biodegradable bio-based aliphatic thermoplastic. In hindsight it can be concluded that despite the efficacy of the optimisation routines, a more careful selection of target variable would have been pertinent.

## Chapter 3 – Research Intended

One of the key elements restricting both the rate of optimisation and wider practicality of the BBAPTs studied this year was the long curing process. This makes their incorporation into composite materials such as those used in wind turbine blades unfavourable due to low throughput rates when compared to contemporary thermosets. An alternative form of thermoset with substantially faster cure times are cross-linked unsaturated polyester systems, these rely upon a combination of condensation and addition polymer. The condensation polymer is typically an unsaturated linear polyester formed from the copolymerisation of diols and diacids, with at least one monomer having an unsaturated double bond in its structure which is retained after copolymerisation- this copolymer is referred to as an unsaturated polyester (UP) (80). The addition polymer is typically generated through a radical-addition homopolymerisation reaction, where a monomer which had been acting as an UP solvent reacts and crosslinks individual UP chains- these monomers are therefore referred to as reactive diluents (RD) (81). When UP and RD are brought together, they are known as unsaturated polyester resin (UPR), a viscous liquid which, on addition of radical-initiating chemicals, can rapidly form a rigid thermoset material (82). Given their rapid curing, low cost, and high strengths, crosslinked UPRs have become ubiquitous, with common composites such as glass fibre reinforced polymers (GFRPs) making use of this class of thermosets (83). GFRP enjoys widespread use in wind turbine blades due to its high tensile strength to weight ratio (84), but due to the crosslinked nature of the thermosetting polymers, blades are hard to recycle. Additionally, when thermal methods are used to recycle these blades the thermoset matrix is invariably combusted (85); since the thermosets employed in GFRP are oil-derived this makes their combustion an emission of fossil carbon to the atmospheric reservoir in the form of CO<sub>2</sub>. Given that non-biodegradable bio-based plastics have been identified as a potential carbon negative solution that would complement the wider circular plastics effort in the run up to the 2050 targets (86), the PhD's fundamental working hypothesis posited to be investigated is this: "Bayesian optimisation can be used to sample-efficiently optimise desirable properties in bio-based thermosets, providing a sustainable solution for wind turbine blade manufacture". The remainder of this PhD project is split into three work packages (corresponding to chapters of the final thesis); firstly, design of an UP synthesis technique and optimisation for high molecular weight product will be investigated. Secondly, design of a bio-based RD synthesis technique is to be carried out before yields are optimised for. Finally, UPR thermosets are to be cured from UPR with a multi-objective optimisation targeting strength and abiotic biodegradability.

### 3.1 – Mono-objective Bio-based UP Synthesis Optimisation

Work package 1 (tasks 1:1-1:6, see Figure 23) concerns the development of a method for the synthesis of unsaturated polyester (UP), and the subsequent mono-objective Bayesian optimisation for the maximisation of chain-length in these UPs- these can be deduced from viscosity measurements (A 17). This chapter investigates the question of whether it is possible for Bayesian optimisation to guide the synthesis of UP.

Initially, a synthesis reactor capable of facilitating polyesterification reactions must be constructed (task 1:1, Figure 23), this can be carried out alongside the development of a characterisation method for chain length estimation from viscosity measurements (task 1:2, Figure 23). Equipment necessary for these tasks has been considered and only an overhead stirrer is missing, this is considered affordable within the project budget- additionally, synthesis reactor setups have been offered by the Lapkin group which may be suitable for these purposes.

Towards the end of these tasks, the coding of programs capable of guiding an experimentalist through Bayesian optimisation of UP manufacture will be engaged with (task 1:3, Figure 23). From experience gained in the 1<sup>st</sup> year's work, a period has been allotted to the

debugging of this program, as gaps in the interface between computational and laboratory techniques are bridged (task 1:4, Figure 23), this component of work can begin as soon as the bulk of the code has been written and is therefore expected to be carried out alongside task 1:3.

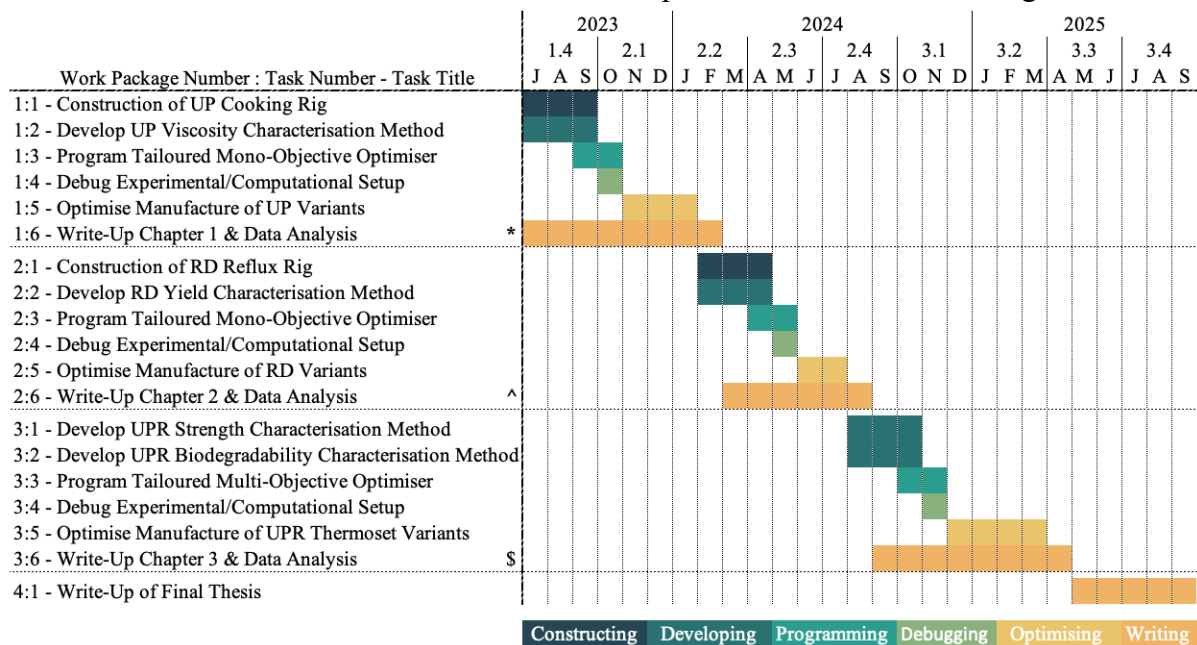


Figure 23 – Time-planning for the fulfilment of work packages 1-3 and their associated tasks.

Subsequently, Bayesian optimisation is practically realised- this will involve the optimisation of three proposed variants of UP- conventional UP (C-UP), partially bio-based UP (PB-UP), and bio-based UP (B-UP) (See Figure 24). C-UP will be synthesised from polyesterification of propylene glycol, maleic acid, and phthalic acid, whilst PB-UP manufacture will involve replacing the unsaturated maleic acid with itaconic acid (87). Finally, B-UP would replace both maleic and phthalic acid with itaconic and 2,5-furandicarboxylic acid respectively (88). Given that an UP can be cooked and characterised in a working day, a month has been set aside for the optimisation of each of these variants (task 1:5, Figure 23)- this is reasonable as an 8 sample space-filling prior dataset can be prepared in a week and a half and further sequential sampling can be carried out for the rest of the month (+20 samples). Writing up of this PhD thesis chapter concerning work package 1 can begin from the outset right through to the conclusion of this work package (task 1:6, Figure 23), and can be re-engaged with if necessary in the final write up period set aside (task 4:1, Figure 23).

Since the projects envisioned are linear in structure due to the nature of optimisation problems and their setup, mitigatory measures have been considered (as noted by the \* in the Gantt chart, Figure 23). In the case that the specified UP formulations fail to polycondense as hoped there are papers which detail commonly practiced methods for the polymerisation of similar but less novel bio-based UP resins, this allows the research question in Chapter 1 to still be addressed (89). In the unlikely event of failure to synthesise any UP whatsoever, commercial routes exist for the acquisition of conventional and partially bio-based UPs which can be used to answer the ultimate research question asked in Chapter 3.

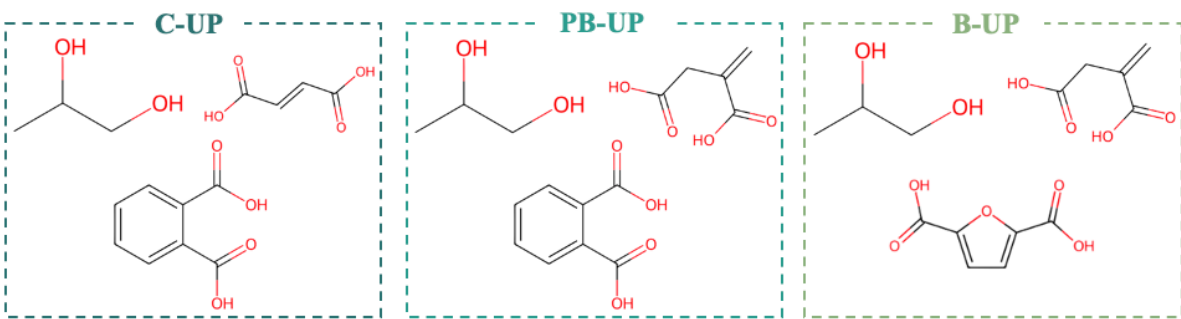


Figure 24 – Overview of the feedstocks to be used in the manufacture of the three UP variants.

### 3.2 – Mono-objective Bio-based RD Synthesis Optimisation

Work package 2 (tasks 2:1-2:6, see Figure 23) concerns the development of a method for the synthesis of reactive diluent (RD), and the subsequent mono-objective Bayesian optimisation for the maximisation of RD yield. The conventional RD (C-RD) styrene can be replaced by the diethyl itaconate (87); synthesised from itaconic acid and ethanol, both which can be bio-based in origin (90-92), yielding a fully bio-based reactive diluent (B-RD) (See Figure 25). The main research question of this chapter will be whether Bayesian optimisation can be leveraged to improve yield of this B-RD given a set of input parameters. A secondary question would be whether the scarcely documented itaconate family member with the IUPAC name 4-O-ethyl 1-O-methyl 2-methylidenebutanedioate could be synthesised; might this be a more suitable alternative to either dimethyl itaconate or diethyl itaconate RDs?



Figure 25 – Overview of reactive diluents to be used. C-RD: Conventional reactive diluent, B-RD: Bio-based reactive diluent.

Initially, a refluxing reactor will be constructed, a rotary evaporator prepared, and separating funnels mounted so that monomers of the itaconate family can be synthesised and isolated (task 2:1, Figure 23) all this equipment is available in the laboratory and chemical feedstocks required are relatively cheap (ethanol and itaconic acid). Method for quantification of yield will be developed in parallel (task 2:2, Figure 23), providing a target variable for later optimisation.

As with work package 1, a period of programming (task 2:3, Figure 23) and debugging (task 2:4, Figure 23) are set aside to allow for the development of a suitable computational/laboratory workflow. Since the refluxing and isolation steps are expected to take a day each it will take around 2 weeks to generate an 8-sample space-filling prior dataset for optimisation. The subsequent sequential sampling procedure will be carried out for a month and a half thereafter to generate a further 20 samples. The yield quantification step can be done in the downtime between periods of refluxing. In total 2 months are therefore set aside for the optimisation of diethyl itaconate yield (task 2:5, Figure 23). Write-up of the associated 2<sup>nd</sup> thesis chapter will be engaged with throughout this work package (task 2:6, Figure 23).

As with chapter 1, mitigatory measures have been considered (noted ^ in the Gantt chart). In the event that the more complicated synthesis of 4-O-ethyl 1-O-methyl 2-methylidenebutanedioate fails, the simpler diethyl itaconate can be returned to, this still allows the main research question of Chapter 2 to be addressed. If neither of the two bio-based RDs can be synthesised in the lab the return to the commercially available styrene still allows the partially bio-based UPRs to be synthesised and the core research question of Chapter 3 to be addressed.

### 3.3 – Multi-objective Bio-based UPR Thermoset Curing Optimisation

Work package 3 (tasks 3:1-3:6, see Figure 23) concerns the development of a method for the curing of unsaturated polyester resin (UPR) into solid thermoset materials, and the subsequent multi-objective Bayesian optimisation for the maximisation of mechanical strength and non-biodegradability. The primary research question to be answered here is whether Bayesian optimisation can be used to create (partially/fully) bio-based UPRs which exhibit the same degree of mechanical performance and resistance to degradation shown by conventional UPRs.

Initially, method needs developing for the characterisation of cured thermoset materials, this includes the quantification of mechanical strength (task 3:1, Figure 23) and abiotic biodegradability (task 3:2, Figure 23) in two separate metrics that will later serve as target variables for multi-objective optimisation. A tensile strength testing machine would be used to obtain tensile/compressive strengths and moduli, whilst a lab-based method would have to be developed for the accelerated quantification of susceptibility to surface erosion.

As with the previous work packages, time is set aside for the subsequent programming (task 3:3, Figure 23) and debugging (task 3:4, Figure 23) of the computational/laboratory workflow for the optimisation task.

Six variants of UPR will be produced based on the three UP variants, a conventional RD, and a bio-based RD. These 6 UPR variants will therefore be optimised simultaneously in 6 separate sequential procedures. Given that curing and characterisation of a 6 sample variant set will take around a day, an 8 sample prior dataset can be generated in a week and a half. Since this is the final and most critical optimisation of the project, an extended period of four months has been allowed for this task (task 3:5, Figure 23). Write-up of the 3<sup>rd</sup> thesis chapter will take place throughout work package 3 (task 3:6, Figure 23).

Mitigatory measures for Chapter 3 were considered (noted \$ in the Gantt chart); in the event of multi-objective optimisation implementation failure a return to a single-objective optimisation could be feasible and the primary research question adapted accordingly.

Work package 4 (task 4:1, see Figure 23) concerns the writing-up of the final thesis, 5 months have been allotted for this purpose.

## 4.0 – Appendix

### 4.1 – Preliminary Experimental Work Appendix

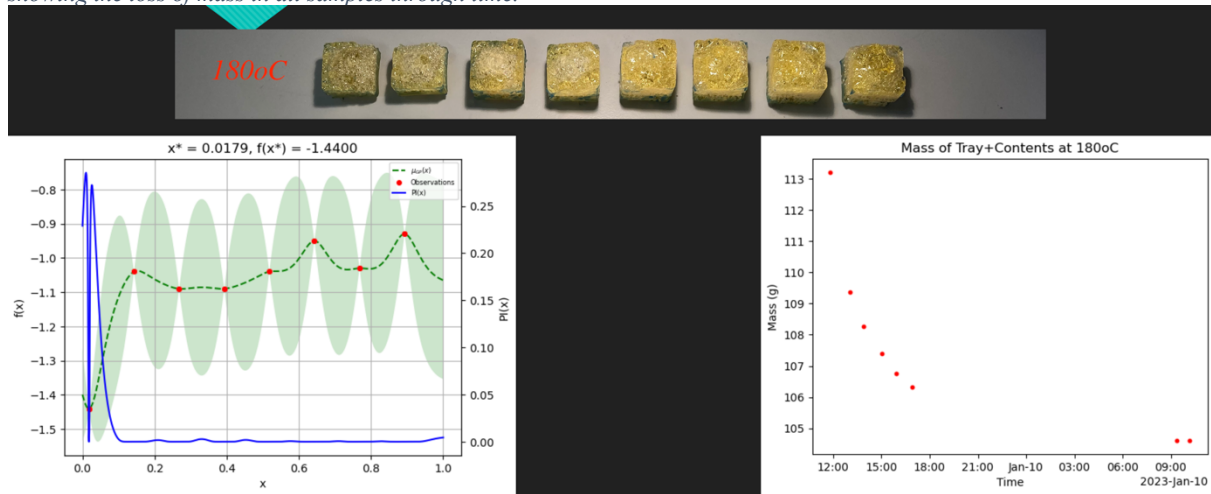
A 1 – Birds-eye view of solid thermoset samples prepared of poly(glycerol itaconic acid) at various drying oven temperatures. Organised by drying oven temperature in the y-axis and ratio of glycerol to itaconic acid in the x-axis.



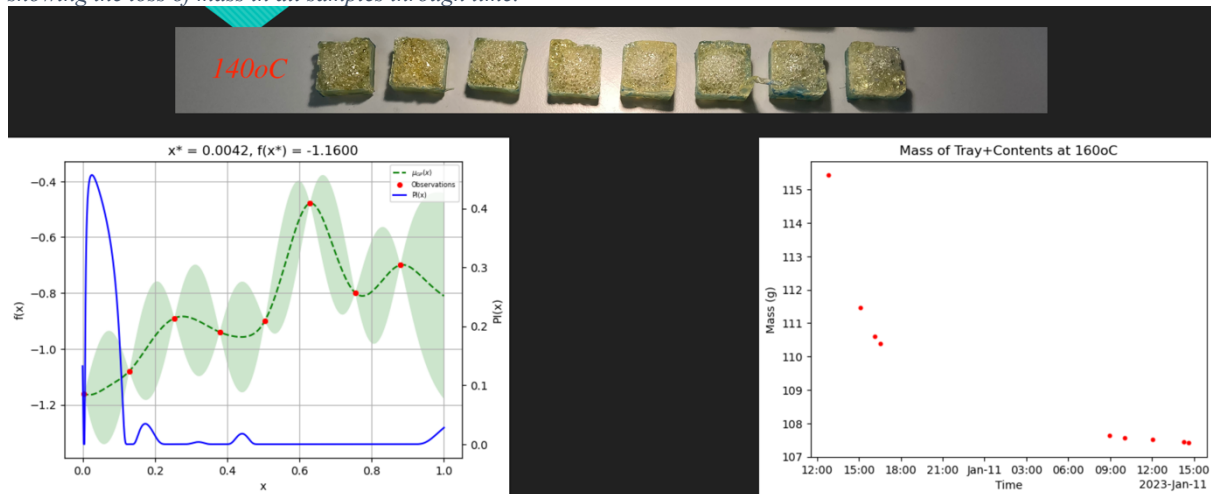
A 2 – Profile view of solid thermoset samples prepared of poly(glycerol itaconate) at various drying oven temperatures.



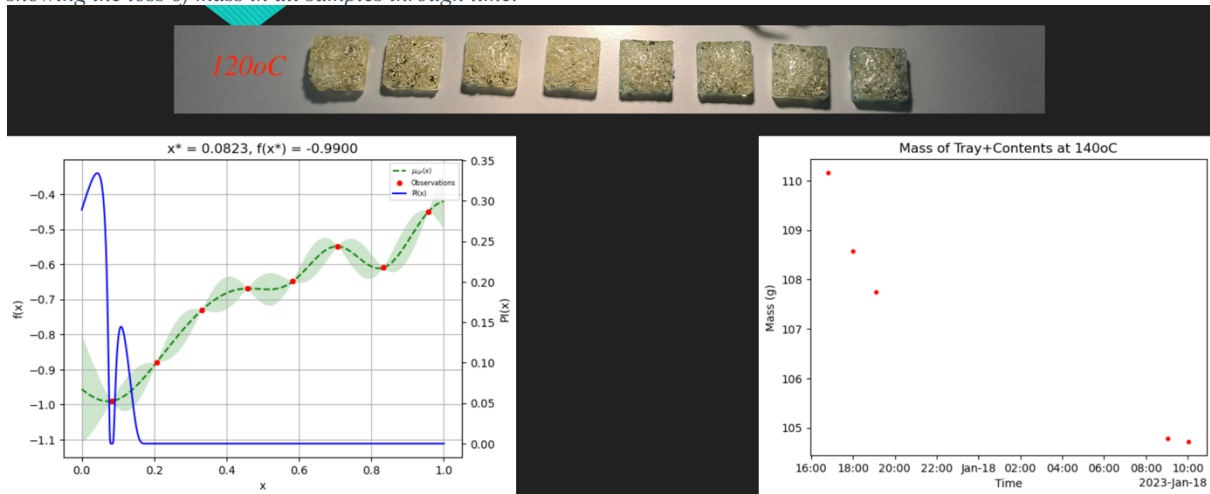
A 3 – Poly(Glycerol Itaconate) samples prepared at 180oC. Top: Image of samples. Left: Plot showing mass loss ( $f(x)$ ) as a function of itaconic acid's normalised stoichiometric ratio ( $x$ ), i.e. where glycerol : itaconic acid is 1: $x$ . Right: Scatter plot showing the loss of mass in all samples through time.



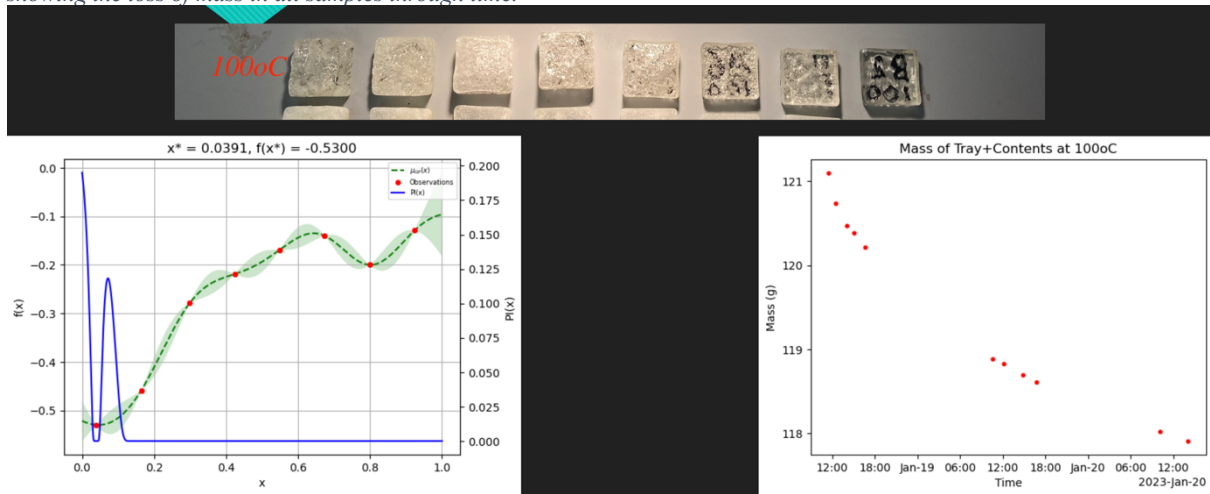
A 4 - Poly(Glycerol Itaconate) samples prepared at 140oC. Top: Image of samples. Left: Plot showing mass loss ( $f(x)$ ) as a function of itaconic acid's normalised stoichiometric ratio ( $x$ ), i.e. where glycerol : itaconic acid is 1: $x$ . Right: Scatter plot showing the loss of mass in all samples through time.



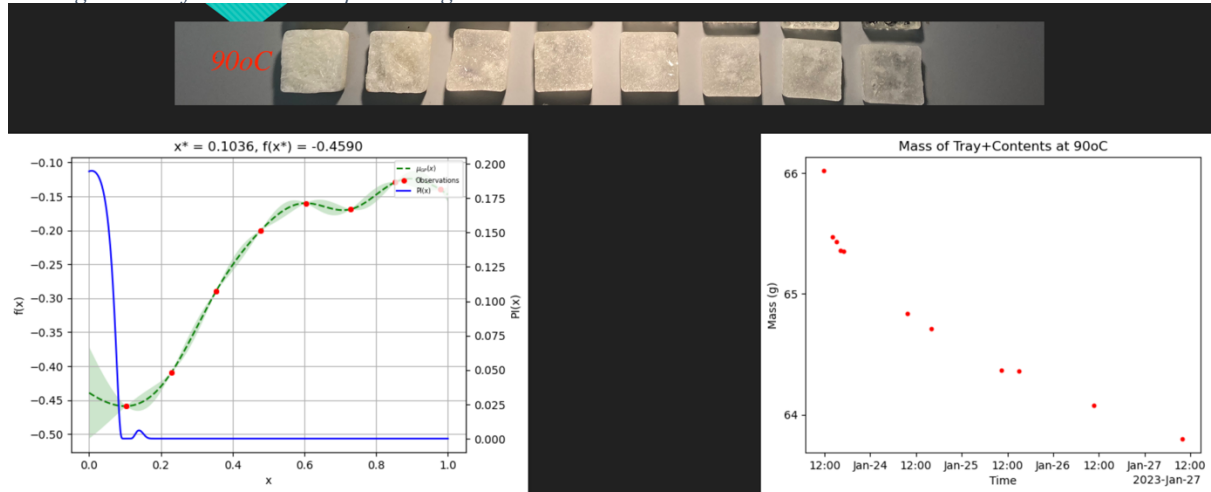
A 5 - Poly(Glycerol Itaconate) samples prepared at 120oC. Top: Image of samples. Left: Plot showing mass loss ( $f(x)$ ) as a function of itaconic acid's normalised stoichiometric ratio ( $x$ ), i.e. where glycerol : itaconic acid is 1: $x$ . Right: Scatter plot showing the loss of mass in all samples through time.



A 6 - Poly(Glycerol Itaconate) samples prepared at 100oC. Top: Image of samples. Left: Plot showing mass loss ( $f(x)$ ) as a function of itaconic acid's normalised stoichiometric ratio ( $x$ ), i.e. where glycerol : itaconic acid is 1: $x$ . Right: Scatter plot showing the loss of mass in all samples through time.

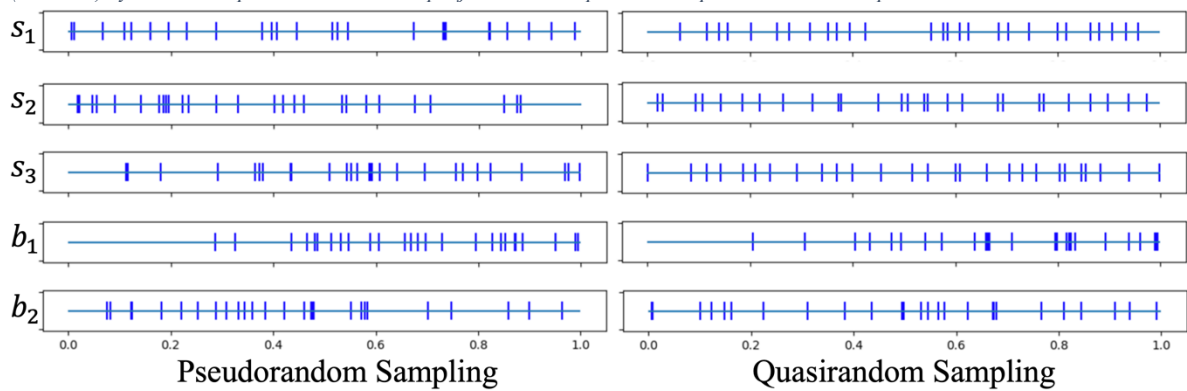


A 7 - Poly(Glycerol Itaconate) samples prepared at 90oC. Top: Image of samples. Left: Plot showing mass loss ( $f(x)$ ) as a function of itaconic acid's normalised stoichiometric ratio ( $x$ ), i.e. where glycerol : itaconic acid is 1: $x$ . Right: Scatter plot showing the loss of mass in all samples through time.

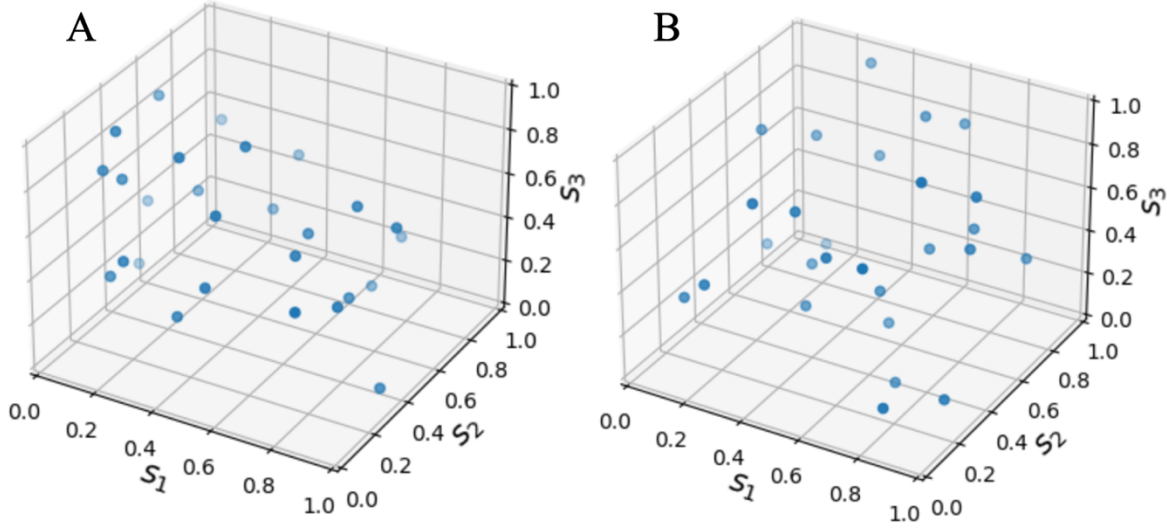


## 4.2 – BBAPT Optimisation Problem Framing Appendix

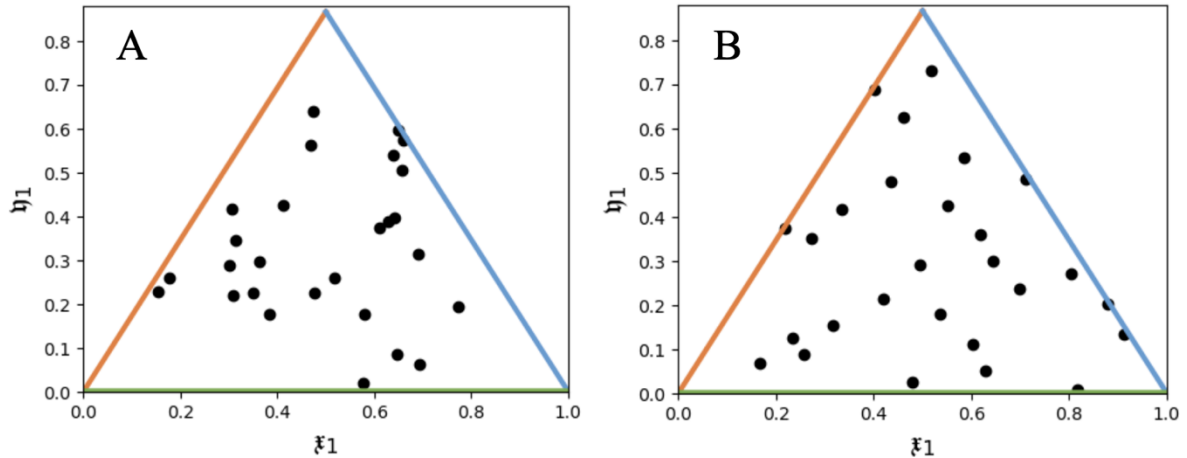
A 8 – Comparison of pseudorandom sampling coverage versus custom quasirandom sampler programmed for 5D P(GCiItSu) system. All 5 predictor variables projected into separate 1D spaces, and 27 samples drawn.



A 9 – Comparison of pseudorandom sampling coverage (A) versus custom quasirandom sampler (B) programmed for 5D P(GCiItSu) system. All three strength predictor variables projected into 3D space, and 27 samples drawn.



A 10 – Comparison of pseudorandom sampling coverage (A) versus custom quasirandom sampler (B) programmed for 5D P(GCiItSu) system. Both balancing predictor variables projected into their 2<sup>nd</sup> order simplex sub-space, and 27 samples drawn.

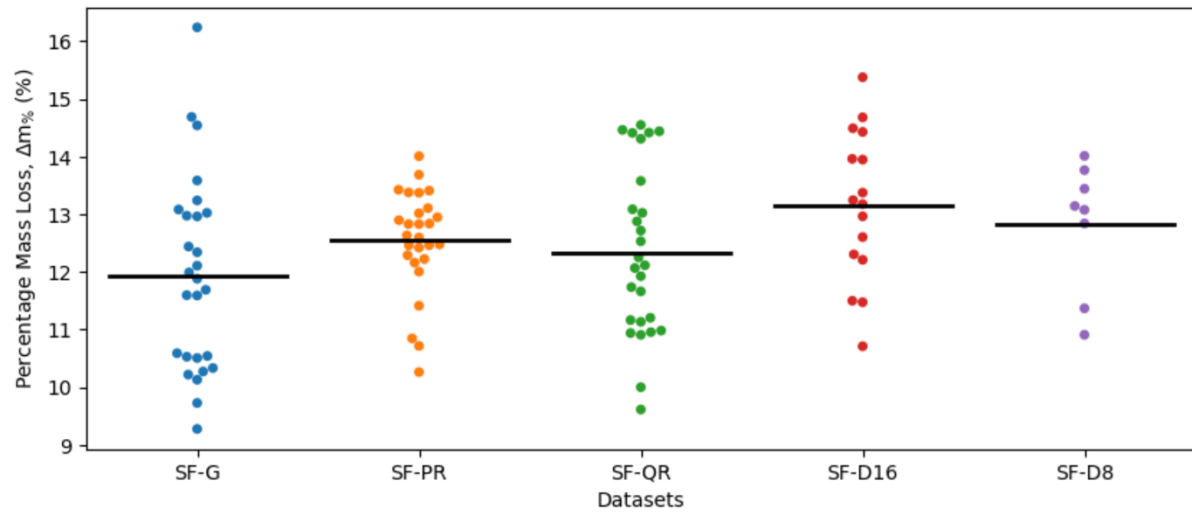


#### 4.3 – P(GCiIt) System Optimisation Appendix

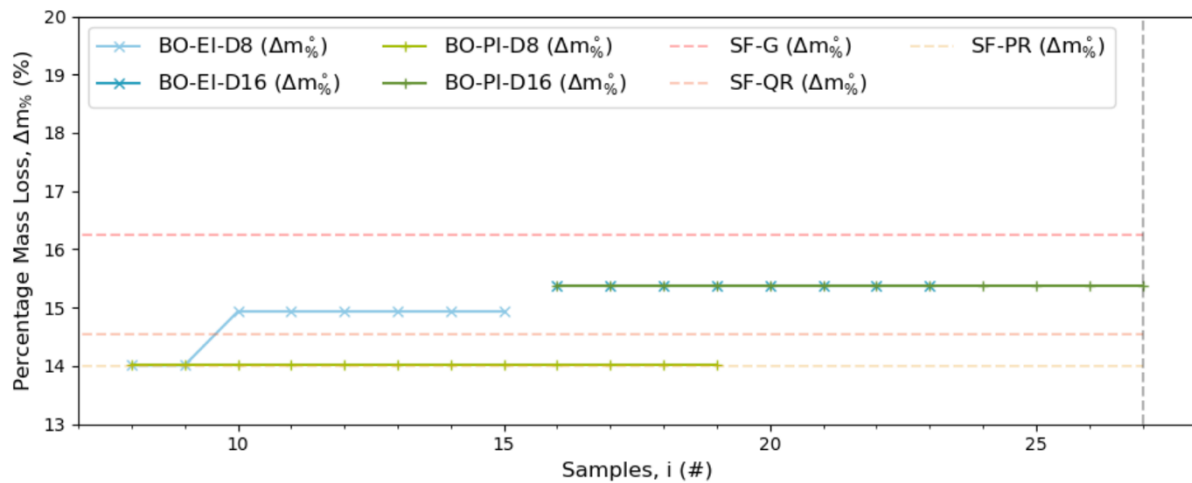
A 11 - Overview of Bayesian optimisation results with respect to the targets obtained after 27 samples (excl. SF-D8 and SF-D16 with 8 and 16 samples respectively). INCLUDES THE EXTRA RESULTS OBTAINED AFTER THE 27 SAMPLE LIMIT. SF: Space-filling method. BO: Bayesian optimisation method. D8/16: 8/16-sample representative dataset. PI: Probability of improvement acquisition function. EI: Expected improvement acquisition function. SF-D8/16: Prior-initialising space-filling datasets are also included here.

Test	Sequential Samples (#)	Max Targets, $\Delta m_{\%}^*$ (%)	Mean of Targets, $\mu_{f(X)}$ (%)	Standard Deviation of Targets, $\sigma_{f(X)}$ (%)
SF-D8	n/a	14.01	12.82	1.04
SF-D16	n/a	15.38	13.15	1.26
BO-PI-D8	19	20.78	12.95	2.33
BO-EI-D8	19	17.99	13.67	1.91
BO-PI-D16	11	15.38	12.76	1.28
BO-EI-D16	11	15.74	13.16	1.57

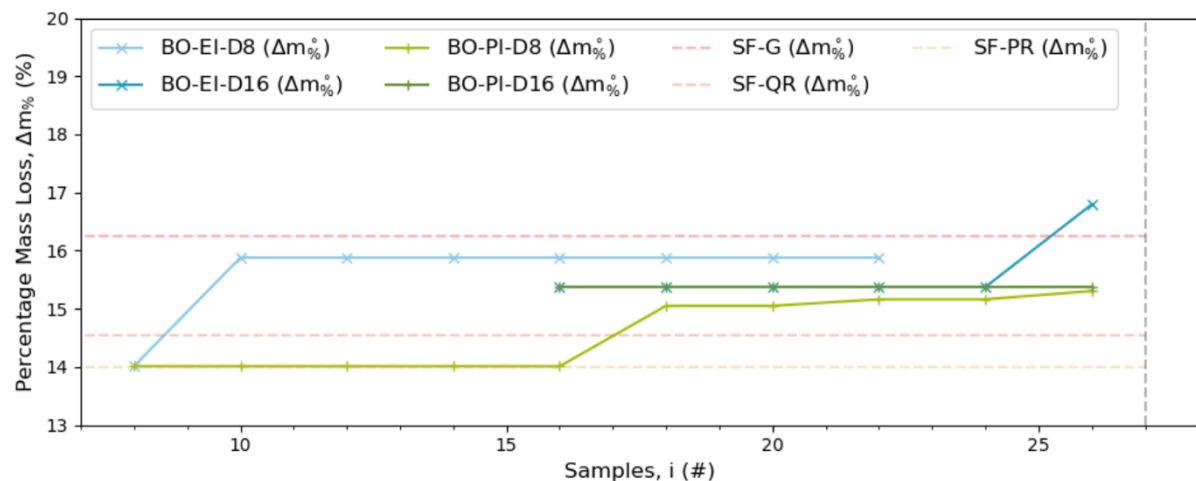
A 12 – Swarm plots showing distributions of data sampled for each of the datasets generated using the space filling techniques. Mean of each dataset is shown as a horizontal black line.



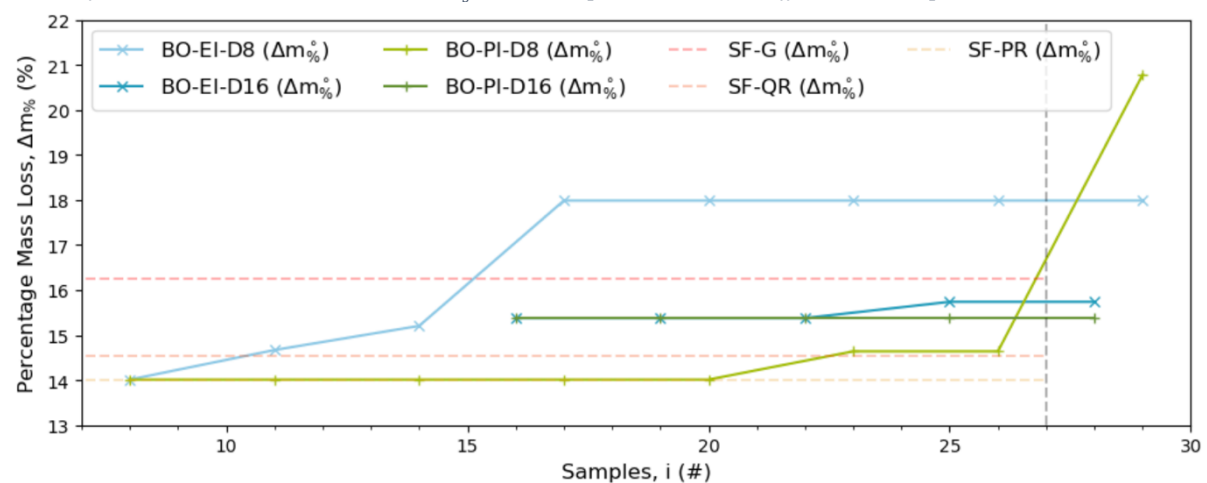
A 13 – Graph describing optimisation progression with respect to best global optimum  $\Delta m^\circ$  discovered at any given iteration for BO-EI-D8 and BO-PI-D8 where  $N_s^i = 1$ . Incomplete optimisation.



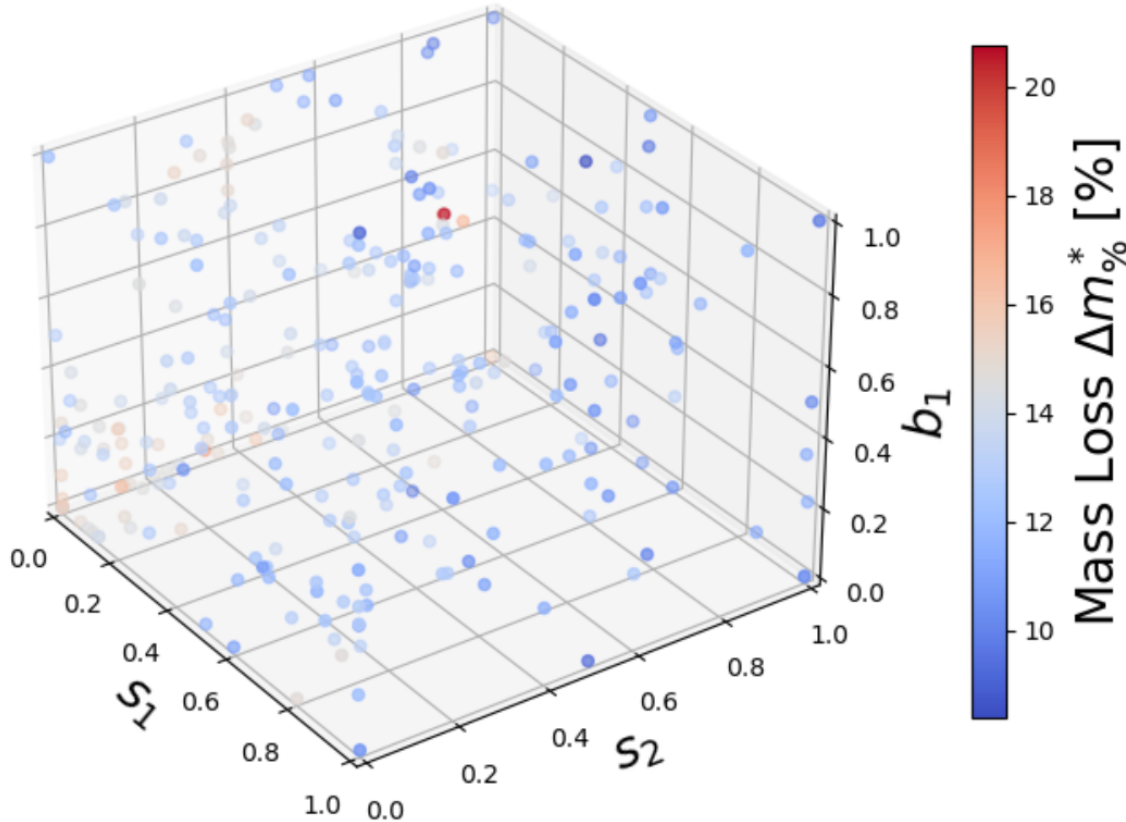
A 14 - Graph describing optimisation progression with respect to best global optimum  $\Delta m^\circ$  discovered at any given iteration for BO-EI-D8 and BO-PI-D8 where  $N_s^i = 2$ . Incomplete optimisation.



A 15 - Graph describing optimisation progression with respect to best global optimum  $\Delta m^\circ$  discovered at any given iteration for BO-EI-D8 and BO-PI-D8 where  $N_s^i = 3$ . Full optimisation, uncut-off at the 27 sample mark.



A 16 – Entire dataset (292 samples across parameter space) describing link between normalised predictor variables  $s_1, s_2, b_1$  and target variable  $\Delta m\%$  in the P(GCilt) system.



A 17 – Connecting viscosity measurements and chain lengths for linear polyesters.

One inherent characteristic of resins is their viscosity, which is an indicator of how long the linear polyester chains are on average. This metric is formally described as the viscosity averaged molecular weight, whose values tend to lie somewhere between what would be the number and weight averaged molecular weights (93). It is calculated using the Mark-Houwink equation (Eq. 49), which links viscosity averaged molecular weight  $M$  with intrinsic viscosity  $[\eta]$  using constants  $k$  and  $a$ . It is a useful metric as dynamic viscosity measurements are easy to make (relative to more complicated methods used to deduce number or weight average molecular weights for resins) and these values can be converted to intrinsic viscosities in a straightforward manner.

$$[\eta] = kM^a \quad \text{Eq. 49}$$

Unfortunately, the Mark-Houwink equation is part of a ‘relative’ method as it relies upon constants determined by ‘absolute’ methods. Absolute methods such as gel permeation chromatography accurately determine the distribution of molecular weights and thereby provide the number and weight average molecular weight values. If a sample were to be sent off for analysis by gel permeation chromatography, then this information could be used to calibrate the Mark-Houwink equation constants, and thereafter avoid the need for further chromatography for viscosity averaged molecular weight determination. If the above method could be developed for UPR characterisation, viscosity averaged molecular weight could provide a useful predictor or constant variable within the wider optimisation experiments carried out. Note, this technique has not had a formal amount of time allotted to it within the

Gantt chart; if this metric were to be considered a constant variable, then it would likely be enough to standardise the viscosity of samples generated.

## 5.0 – Acknowledgements

This work was supported by the UKRI Centre for Doctoral Training in Application of Artificial Intelligence to the study of Environmental Risks (reference EP/S022961/1).

## 6.0 – Bibliography

1. IPCC. Climate Change 2014: Synthesis Report. Contribution of Working Groups I, II and III to the Fifth Assessment Report of the Intergovernmental Panel on Climate Change. Geneva, Switzerland: Intergovernmental Panel on Climate Change; 2014.
2. Ritchie H, . et al. CO<sub>2</sub> and greenhouse gas emissions Our World in Data Website: Our World in Data; 2020 [Available from: <https://ourworldindata.org/emissions-by-sector#citation>].
3. Levi P, et al. Mapping global flows of chemicals: from fossil fuel feedstocks to chemical products. *Environmental Science & Technology*. 2018;52:1725-34.
4. OECD. Global Plastics Outlook: Economic Drivers, Environmental Impacts and Policy Options. Paris: OECD Publishing; 2022.
5. Millican JM, Agarwal S. Plastic Pollution: A Material Problem? *Macromolecules*. 2021;54(10):4455-69.
6. Yuan Z, et al. Ranking of potential hazards from microplastics polymers in the marine environment. *Journal of Hazardous Materials*. 2022;429.
7. Zhang S, Wang J, Liu X, Qu F, Wang X, Wang X, et al. Microplastics in the environment: A review of analytical methods, distribution, and biological effects. *TrAC Trends in Analytical Chemistry*. 2019;111:62-72.
8. Zhang Y, Kang S, Allen S, Allen D, Gao T, Sillanpää M. Atmospheric microplastics: A review on current status and perspectives. *Earth-Science Reviews*. 2020;203:103118.
9. Schneiderman DK, Hillmyer MA. 50th Anniversary Perspective: There Is a Great Future in Sustainable Polymers. *Macromolecules*. 2017;50(10):3733-49.
10. Post W, Susa A, Blaauw R, Molenveld K, Knoop RJI. A Review on the Potential and Limitations of Recyclable Thermosets for Structural Applications. *Polymer Reviews*. 2020;60(2):359-88.
11. Pickering S. Recycling technologies for thermoset composite materials- current status. *Composites Part A: Applied Science and Manufacturing*. 2005;37:1206-15.
12. Yang Y, et al. Recycling of composite materials. *Chemical Engineering and Processing*. 2012;51:53-68.
13. Chen J, et al. Recycling and reuse of composite materials for wind turbine blades: An overview. *Reinforced Plastics & Composites*. 2019;38:567-77.
14. WCED. Our Common Future. The United Nation's World Commission on Environment and Development; 1987.
15. UN. The 2030 Agenda for Sustainable Development. United Nations; 2015. Contract No.: A/RES/70/1.
16. Ma S, et al. Degradable thermosets based on labile bonds or linkages: A review. *Progress in Polymer Science*. 2017;76:65-110.
17. Utekar S, et al. Comprehensive study of recycling of thermosetting polymer composites - Driving force, challenges and methods. *Composites Part B*. 2020;207.

18. Beauson J, et al. Recycling of shredded composites from wind turbine blades in new thermoset polymer composites. *Composites: Part A*. 2016;90:390-9.
19. Chen R, et al. Comparative pyrolysis characteristics of representative commercial thermosetting plastic waste in inert and oxygenous atmosphere. *Fuel*. 2019;246:212-21.
20. Liu Y, et al. Closed-loop chemical recycling of thermosetting polymers and their applications: a review. *Green Chemistry*. 2022;24:5691-708.
21. Tesoro G, et al. Reversible Crosslinking in Epoxy Resins. I. Feasibility Studies. *Applied Polymer Science*. 1990;39:1425-37.
22. Bobade S, Paluvai, N., Mohanty, S., Nayak, S. Bio-based thermosetting resins for future generation: a review. *Polymer-Plastics Technology and Engineering*. 2016;55:17:1836-96.
23. Müller R, et al. Biodegradation of polyesters containing aromatic constituents. *Biotechnology*. 2001;86:87-95.
24. Zheng Y, et al. A review of plastic waste biodegradation. *Critical Reviews in Biotechnology*. 2005;25:243-50.
25. Sharma S, et al. A handbook of applied biopolymer technology. Cambridge: RSC Publishing; 2011.
26. Shirahama H, et al. Synthesis and enzymatic degradation of high molecular weight aliphatic polyesters. *Applied Polymer Science*. 2000;80:340-7.
27. Lee S, et al. Microstructure, tensile properties, and biodegradability of aliphatic polyester/clay nanocomposites. *Polymer*. 2002;43:2495-500.
28. Chrissafis K, et al. Thermal degradation kinetics of the biodegradable aliphatic polyester, poly(propylene succinate). *Polymer Degradation and Stability*. 2006;91:60-8.
29. Pranamuda H, et al. Microbial degradation of an aliphatic polyester with a high melting point, poly(tetramethylene succinate). *Applied and Environmental Microbiology*. 1995;61:1828-32.
30. Barrett D, et al. Design and applications of biodegradable polyester tissue scaffolds based on endogenous monomers found in human metabolism. *Molecules*. 2009;14:4022-50.
31. Lee X, et al. Biodegradable and temperature-responsive polyesters with renewable monomers. *Applied Polymer Science*. 2016.
32. Barrett D, et al. Aliphatic polyester elastomers derived from erythritol and a,w-diacids. *Polymer Chemistry*. 2010;1:296-302.
33. Bruggeman J, et al. Biodegradable poly(polyol sebacate) polymers. *Biomaterials*. 2008;29:4726-35.
34. Amsden B. Curable, biodegradable elastomers: emerging biomaterials for drug delivery and tissue engineering. *Soft Matter*. 2007;3:1335-48.
35. Zhang H, et al. Recent advances in glycerol polymers: chemistry and biomedical applications. *Macromolecular Rapid Communications*. 2014;35:1906-24.
36. Álvarez-Chávez C, et al. Sustainability of bio-based plastics: general comparative analysis and recommendations for improvement. *Cleaner Production*. 2012;23:46-56.
37. Rudin A, et al. The elements of polymer science and engineering: Academic press; 2013.
38. Palm E, et al. Electricity-based plastics and their potential demand for electricity and carbon dioxide. *Cleaner Production*. 2016;129:548-55.
39. Tesfamariam S, et al. Handbook of Seismic Risk Analysis and Management of Civil Infrastructure Systems: Woodhead Publishing; 2013.
40. Kuhn R, et al. Chapter One - Combinatorial Testing: Theory and Practice. *Advances in Computers*. 99: Academic Press Inc; 2015. p. 1-66.
41. Anderson M, et al. Design of Experiments. Kirk-Othmer Encyclopedia of Chemical Technology: John Wiley & Sons Inc; 2010.
42. Uy M, et al. Optimization by Design of Experiment Technique. 2009 IEEE Aerospace Conference; Big Sky, MT, USA: IEEE; 2009.

43. Greenhill S, et al. Bayesian optimization for adaptive experimental design: A review. *IEEE Access*. 2020;8:13937-48.
44. Liu H, et al. A survey of adaptive sampling for global metamodeling in support of simulation-based complex engineering design. *Structural and Multidisciplinary Optimisation*. 2018;57:393-416.
45. Garud S, et al. Design of computer experiments: A review. *Computers and Chemical Engineering*. 2017;106:71-95.
46. Perez V, et al. Adaptive experimental design for construction of response surface approximations. *AIAA Journal*. 2002;40:2495-503.
47. Halpern J, et al. A biodegradable thermoset polymer made by esterification of citric acid and glycerol. *Journal of Biomedical Materials Research Part A*. 2013;102(5):1467-77.
48. Alberts AH, Rothenberg G. Plantics-GX: a biodegradable and cost-effective thermoset plastic that is 100% plant-based. *Faraday Discussions*. 2017;202(0):111-20.
49. Bischi B, et al. mlrMBO: A modular framework for model-based optimisation of expensive black-box functions. *Computational Statistics & Data Analysis*. 2018;1-26.
50. Trenkel-Amoroso J. Synthesis, degradation and practical applications of a glycerol/citric acid condensation polymer: Oregon State University; 2008.
51. Shukla K. A study on the synthesis of various polyesters from glycerol. *Journal of Polymer Research*. 2022;29(373).
52. Stork J, et al. A new taxonomy of global optimization algorithms. *Natural Computing*. 2022;21:219-42.
53. Roeva O. Real-world Applications of Genetic Algorithms: InTech; 2012.
54. Li C, Rubín De Celis Leal D, Rana S, Gupta S, Sutti A, Greenhill S, et al. Rapid Bayesian optimisation for synthesis of short polymer fiber materials. *Scientific Reports*. 2017;7(1).
55. Mockus J, et al. The application of bayesian methods for seeking the extremum. *Towards Global Optimisation*. 1978;2:117-28.
56. Jones D, et al. Efficient global optimization of expensive black-box functions. *Journal of Global Optimization*. 1998;13:455-92.
57. Calandra R, et al. Bayesian optimization for learning gaits under uncertainty. *Annals of Mathematics and Artificial Intelligence*. 2016;76:5-23.
58. Bader J, et al. Improving extracellular vesicles production through a Bayesian optimization-based experimental design. *European Journal of Pharmaceutics and Biopharmaceutics*. 2023;182:103-14.
59. Cho H. Basic enhancement strategies when using Bayesian optimization for hyperparameter tuning of deep neural networks. *IEEE Access*. 2020;8:52588-608.
60. Yamashita T, et al. Crystal structure prediction accelerated by Bayesian optimization. *Physical Review Materials*. 2018;2.
61. Balachandran P, et al. Adaptive strategies for materials design using uncertainties. *Scientific Reports*. 2016;6.
62. Karasuyama M, et al. Computational design of stable and highly ion-conductive materials using multi-objective Bayesian optimization: case studies on diffusion of oxygen and lithium. *Computational Materials Science*. 2020;184.
63. Tisserat B, et al. Glycerol citrate polyesters produced through heating without catalysis. *Journal of Applied Polymer Science*. 2012;125:3429-37.
64. Sen S, et al. Quasi-versus pseudo-random generators: discrepancy, complexity and integration-error based comparison. *International Journal of Innovative Computing, Information and Control*. 2006;2:1-31.
65. The pandas development t. *pandas-dev/pandas: Pandas*. 2020.

66. Charles RH, Millman KJ, Stfan JvdW, Ralf G, Pauli V, David C, et al. Array programming with NumPy. *Nature*. 2020;585(7825):357--62.
67. Virtanen P, Gommers R, Oliphant TE, Haberland M, Reddy T, Cournapeau D, et al. SciPy 1.0: Fundamental Algorithms for Scientific Computing in Python. *Nature Methods*. 2020;17:261--72 , adsurl = <https://rdcu.be/b08Wh>.
68. Hunter JD. Matplotlib: A 2D graphics environment. *Computing in Science \& Engineering*. 2007;9(3):90--5.
69. Frazier P. A tutorial on Bayesian optimization. 2018.
70. Facebook-Open-Source. Ax - Adaptive Experimentation Platform Ax Website: Meta Platforms Inc; 2022 [Available from: <https://ax.dev/>].
71. Balandat M, Karrer B, Jiang DR, Daulton S, Letham B, Wilson AG, Bakshy E. BoTorch: A Framework for Efficient Monte-Carlo Bayesian Optimization. *Advances in Neural Information Processing Systems* 332020.
72. Downey A. Think Bayes: O'Reilly Media Inc; 2013.
73. Rasmussen C, et al. Gaussian Processes for Machine Learning: MIT Press; 2005.
74. Deisenroth M, et al. Mathematics for Machine Learning: Cambridge University Press; 2020.
75. Snoek J, Larochelle, H., Adams, R., editor Practical bayesian optimization of machine learning algorithms. *Advances in Neural Information Processing Systems*; 2012: Curran Associates Inc.
76. Kushner H. A new method of locating the maximum point of an arbitrary multipeak curve in the presence of noise. *Journal of Basic Engineering*. 1964;86:97-106.
77. Srinivas N, et al. Gaussian process optimization in the bandit setting: no regret and experimental design. *Proceedings of the 27th International Conference on Machine Learning2010*.
78. Siivola E, et al. Preferential batch Bayesian optimization. 2003.
79. Højlund-Dodd T. BO4BT Github Website: ThomasDodd97; 2023 [Available from: <https://github.com/ThomasDodd97/BO4BT>].
80. Seraji S, et al. Fire-retardant unsaturated polyester thermosets: The state-of-the-art, challenges and opportunities. *Chemical Engineering Journal*. 2022;430.
81. Chen J, et al. Synthesis and application of polyepoxide cardanol glycidyl ether as biobased polyepoxide reactive diluent for epoxy resin. *ACS Sustainable Chemistry & Engineering*. 2015;3:1164-71.
82. An W, et al. Chemical recovery of thermosettingunsaturated polyester resins. *Green Chemistry*. 2022;24:710-2.
83. Karatas M, et al. A review on machinability of carbon fiber reinforced polymer (CFRP) and glass reinforced polymer (GFRP) composite materials. *Defence Technology*. 2018;14:318-26.
84. Jensen J, et al. Wind turbine blade recycling: Experiences, challenges and possibilities in a circular economy. *Renewable and Sustainable Energy Reviews*. 2018;97:165-76.
85. Kalkanis K, et al. Wind turbine blade composite materials - end of life treatment methods. *Energy Procedia*. 2019;157:1136-43.
86. Stegmann P, et al. Plastic futures and their CO<sub>2</sub> emissions. *Nature*. 2022;612:272-6.
87. Panic V, et al. Simple one-pot synthesis of fully biobased unsaturated polyester resins based on itaconic acid. *Biomacromolecules*. 2017;18:3881-91.
88. Dai J, et al. 2,5-Furandicarboxylic acid - and itaconic acid-derived fully biobased unsaturated polyesters and their cross-linked networks. *Industrial & Engineering Chemistry Research*. 2017;56:2650-7.
89. Hofmann M, et al. Biobased thermosetting polyester resin for high-performance applications. *ACS Sustainable Chemistry & Engineering*. 2022;10:3442-54.

90. Cowie J. Physical properties of polymers based on itaconic acid. *Pure & Applied Chemistry*. 1979;51:2331-43.
91. Cowie J, et al. Poly(alkyl itaconates): 4. Glass and sub-glass transitions in the di-alkyl ester series, methyl to hexyl. *Polymer*. 1977;18:612-6.
92. Domínguez E, et al. A series of mono and diesters of itaconic acid: synthesis and structural determination. *Monatsefte für Chemie*. 1989;120:743-8.
93. Brazel C, Rosen, S. *Fundamental Principles of Polymeric Materials*: Wiley; 2012.